Please cite this article in press as: Yao et al., Coordinated regulation of plant immunity by poly(ADP-ribosyl)ation and K63-linked ubiquitination, Molecular Plant (2021), https://doi.org/10.1016/j.molp.2021.08.013

Molecular Plant
Research article

CellPress
Partner Journal

Coordinated regulation of plant immunity by poly(ADP-ribosyl)ation and K63-linked ubiquitination

Dongsheng Yao[1], Marcus A. Arguez[1], Ping He[2], Andrew F. Bent[3] and Junqi Song[1,4,*]

[1]Texas A&M AgriLife Research Center at Dallas, Texas A&M University System, Dallas, TX 75252, USA

[2]Department of Biochemistry and Biophysics, Texas A&M University, College Station, TX 77843, USA

[3]Department of Plant Pathology, University of Wisconsin-Madison, Madison, WI 53706, USA

[4]Department of Plant Pathology and Microbiology, Texas A&M University, College Station, TX 77843, USA

***Correspondence: Junqi Song (junqi.song@ag.tamu.edu)**

https://doi.org/10.1016/j.molp.2021.08.013

ABSTRACT

Poly(ADP-ribosyl)ation (PARylation) is a posttranslational modification reversibly catalyzed by poly(ADP-ribose) polymerases (PARPs) and poly(ADP-ribose) glycohydrolases (PARGs) and plays a key role in multiple cellular processes. The molecular mechanisms by which PARylation regulates innate immunity remain largely unknown in eukaryotes. Here we show that Arabidopsis UBC13A and UBC13B, the major drivers of lysine 63 (K63)-linked polyubiquitination, directly interact with PARPs/PARGs. Activation of pathogen-associated molecular pattern (PAMP)-triggered immunity promotes these interactions and enhances PARylation of UBC13. Both *parp1 parp2* and *ubc13a ubc13b* mutants are compromised in immune responses with increased accumulation of total pathogenesis-related (PR) proteins but decreased accumulation of secreted PR proteins. Protein disulfide-isomerases (PDIs), essential components of endoplasmic reticulum quality control (ERQC) that ensure proper folding and maturation of proteins destined for secretion, complex with PARPs/PARGs and are PARylated upon PAMP perception. Significantly, PARylation of UBC13 regulates K63-linked ubiquitination of PDIs, which may further promote their disulfide isomerase activities for correct protein folding and subsequent secretion. Taken together, these results indicate that plant immunity is coordinately regulated by PARylation and K63-linked ubiquitination.

Key words: UBC13, PARP1, PARP2, PDI, poly(ADP-ribosyl)ation, K63-linked ubiquitination, secretory pathway, PAMP-triggered immunity, systemic acquired resistance

Yao D., Arguez M.A., He P., Bent A.F., and Song J. (2021). Coordinated regulation of plant immunity by poly(ADP-ribosyl)ation and K63-linked ubiquitination. Mol. Plant. **14**, 1–16.

INTRODUCTION

Plants possess sophisticated immune systems to protect themselves from invading pathogens (Spoel and Dong, 2012). The first layer of plant innate immunity is mediated by cell surface–localized pattern recognition receptors (PRRs) that recognize the highly conserved pathogen-associated molecular patterns (PAMPs) to initiate pattern-triggered immunity (PTI) (Boller and Felix, 2009). A robust second layer of immunity is effector-triggered immunity (ETI) mediated by nucleotide-binding leucine-rich repeat (NLR) immune receptors, after direct or indirect recognition of pathogen effectors (Jones and Dangl, 2006). The Arabidopsis receptor kinase FLS2 is a well-characterized PRR, which recognizes a conserved 22-amino-acid peptide (flg22) from the N-terminal domain of bacterial flagellin (Gomez-Gomez and Boller, 2000) and triggers immune responses, including production of reactive oxygen species (ROS), activation of mitogen-activated protein kinases (MAPKs), and callose deposition (Boller and Felix, 2009; Dodds and Rathjen, 2010; Macho and Zipfel, 2014). Flg22 treatment also led to the accumulation of signaling molecule salicylic acid (SA) and increased expression of SA-dependent secretory pathway genes and pathogenesis-related genes (*PR*), such as *PR1*, a widely used marker of plant defense responses (Mishina and Zeier, 2007; Denoux et al., 2008; Tsuda et al., 2008). *PR* genes encode small, secreted, or vacuole-targeted proteins with antimicrobial activities (Van Loon and Van Strien, 1999).

Published by the Molecular Plant Shanghai Editorial Office in association with Cell Press, an imprint of Elsevier Inc., on behalf of CSPB and CEMPS, CAS.

Please cite this article in press as: Yao et al., Coordinated regulation of plant immunity by poly(ADP-ribosyl)ation and K63-linked ubiquitination, Molecular Plant (2021), https://doi.org/10.1016/j.molp.2021.08.013

PARylation is a posttranslational protein modification, primarily mediated by poly(ADP-ribose) polymerase (PARP), which transfers ADP-ribose moieties from NAD^+ to acceptor proteins (Gibson and Kraus, 2012). The covalently attached poly (ADP-ribose) polymers on the acceptor proteins can be hydrolyzed by poly(ADP-ribose) glycohydrolase (PARG) (Gibson and Kraus, 2012; Luo and Kraus, 2012). PARylation plays a critical role in diverse cellular processes, including DNA damage repair, chromatin modification, transcription, translation, and cell death. This posttranslational modification has been extensively characterized in humans due to its profound medical impacts in various inflammatory and malignant disorders, including cancers, diabetes, ischemia, and neural diseases, leading to the development of therapeutic PARP inhibitors (Peralta-Leal et al., 2009; Gibson and Kraus, 2012; Bai, 2015; Bock et al., 2015; Gupte et al., 2017). The Arabidopsis genome encodes three PARP proteins, PARP1 (*At2g31320*), PARP2 (*At4g02390*), and PARP3 (*At5g22470*), and two members of PARG proteins, PARG1 and PARG2 (Briggs and Bent, 2011; Lamb et al., 2012). Among the three PARP proteins, PARP2 makes the greatest contribution to PARP activity and organismal viability in response to various genotoxic stresses and bacterial infections (Feng et al., 2015; Song et al., 2015). PARP3 does not appear to have PARP activity due to lack of the highly conserved catalytic residues (Lamb et al., 2012), and its expression is restricted to seed tissues (Rissel et al., 2014). We have previously demonstrated that protein PARylation plays an important role in plant immune gene expression and defense against pathogen attack. Genetic abolishment of *PARP2*, alone or together with *PARP1*, rendered plants more susceptible to the bacterial pathogen *Pseudomonas syringae* pv *tomato* (*Pst*) DC3000 (Feng et al., 2015; Song et al., 2015). In Arabidopsis, PARG1, rather than PARG2, carries the major glycohydrolase activity (Feng et al., 2015; Song et al., 2015), and disruption of *PARG1*, not *PARG2*, altered various plant defense responses (Adams-Phillips et al., 2010). Identification of PARylated proteins is critical to define the function of PARylation in diverse cellular processes. In plants, the roles of PARylation remain largely unexplored, and very few PARP targets have been identified and characterized. A protein array coupled with *in vitro* PARylation assay identified a forkhead-associated domain protein named DAWDLE (DDL), whose PARylation mediated by PARP2 is required for its function in plant immunity (Feng et al., 2016).

Ubiquitination is another posttranslational modification that plays a fundamental role in regulating the function of proteins by altering their stability, localization, and activity (Pickart, 2001; Swatek and Komander, 2016; Zhou and Zeng, 2017; Romero-Barrios and Vert, 2018). The best characterized ubiquitination is mediated by the formation of lysine-48 (K48)-linked polyubiquitin chains, the most abundant linkage type, which targets proteins for degradation through 26S proteasomes (Hochstrasser, 1996). K63-linked ubiquitination represents the second most abundant type of ubiquitin modification and does not usually lead to proteasome-dependent protein degradation, but it fulfills other important roles in DNA damage, autophagy and organelle clearance, innate immunity, and endocytosis in humans and yeast (Andersen et al., 2005, 2008; Nathan and Lehner, 2009; Chen, 2012; Iwai, 2012; Wu and Karin, 2015; Yau and Rape, 2016). UBC13 is a ubiquitin-conjugating enzyme (E2) that exclusively catalyzes the synthesis of noncanonical K63-linked polyubiquitin chains (Hofmann and Pickart, 1999; Pastushok et al., 2005).

Highly homologous UBC13 proteins have been identified in plants with similar roles in DNA damage repair (Wen et al., 2006) and innate immunity (Mural et al., 2013; Turek et al., 2018; Wang et al., 2019). Tomato UBC13 and its cofactor Uev-like protein regulate cell death mediated by a protein kinase Fen and some NLR proteins through K63-linked ubiquitination (Mural et al., 2013). Recently, Arabidopsis UBC13 was also found to be required for PTI and ETI via interaction with an F-box protein CPR1 that regulates the homeostasis of an NLR protein SNC1 (Turek et al., 2018; Wang et al., 2019). In addition, plant UBC13 is also involved in other biological processes, including growth and development (Li and Schmidt, 2010; Wen et al., 2014), iron deficiency response (Li and Schmidt, 2010), metabolism (Deruyffelaere et al., 2015), and low-temperature stress (Wang et al., 2019). To date, only a few K63-ubiquitinated proteins have been identified and functionally characterized in plants, including the auxin efflux carrier PIN2 (Leitner et al., 2012), the boron transporter BOR1 (Kasai et al., 2011), and the brassinosteroid hormone receptor BRI1 (Martins et al., 2015).

Although PARylation and ubiquitination play pivotal roles in a wide variety of cellular processes, the mechanistic link between the two posttranslational modifications remains elusive. Here, we report that UBC13 complexes with PARP1/2 and PARG1/2 and is PARylated upon PAMP elicitation. The *parp* and *ubc13a ubc13b* mutants are more susceptible to *Pst* DC3000, likely due to compromised protein secretory pathway despite an increased accumulation of total antimicrobial PR proteins in these mutants. Furthermore, proteins involved in the secretory pathway, such as protein disulfide isomerases (PDIs), are PARylated upon PAMP treatment. PARylation of UBC13 and PDIs promotes K63-linked ubiquitination of PDIs. We also demonstrated that disruption of the PARP and UBC13 function led to reduced disulfide isomerase activities, indicating that PARylation of PDIs and UBC13 contributes to the activities of PDIs. Our study uncovers a mechanistic interplay of the two fundamental posttranslational modifications in regulating immunity.

RESULTS

UBC13 interacts with PARP1/2 and PARG1/2

To identify the potential PARylated proteins in Arabidopsis, we performed a yeast two-hybrid screen using PARG2 as bait and identified UBC13B. UBC13 is a ubiquitin conjugating enzyme that catalyzes the synthesis of K63-linked polyubiquitin chains (Hofmann and Pickart, 1999; Pastushok et al., 2005). The Arabidopsis genome encodes two *UBC13* genes, namely *UBC13A* (*UBC35*) and *UBC13B* (*UBC36*), with an amino acid identity of 98% to each other and an identity of 79% to human and mouse UBC13. Both *UBC13* genes were able to complement the yeast *ubc13* null mutant with regard to sensitivity to genotoxic agents and spontaneous mutagenesis (Wen et al., 2006). Intriguingly, UBC13 was also identified as a target of Arabidopsis PARP2 and human PARP1 from our previous protein array-based screen (Feng et al., 2016) and

Please cite this article in press as: Yao et al., Coordinated regulation of plant immunity by poly(ADP-ribosyl)ation and K63-linked ubiquitination, Molecular Plant (2021), https://doi.org/10.1016/j.molp.2021.08.013

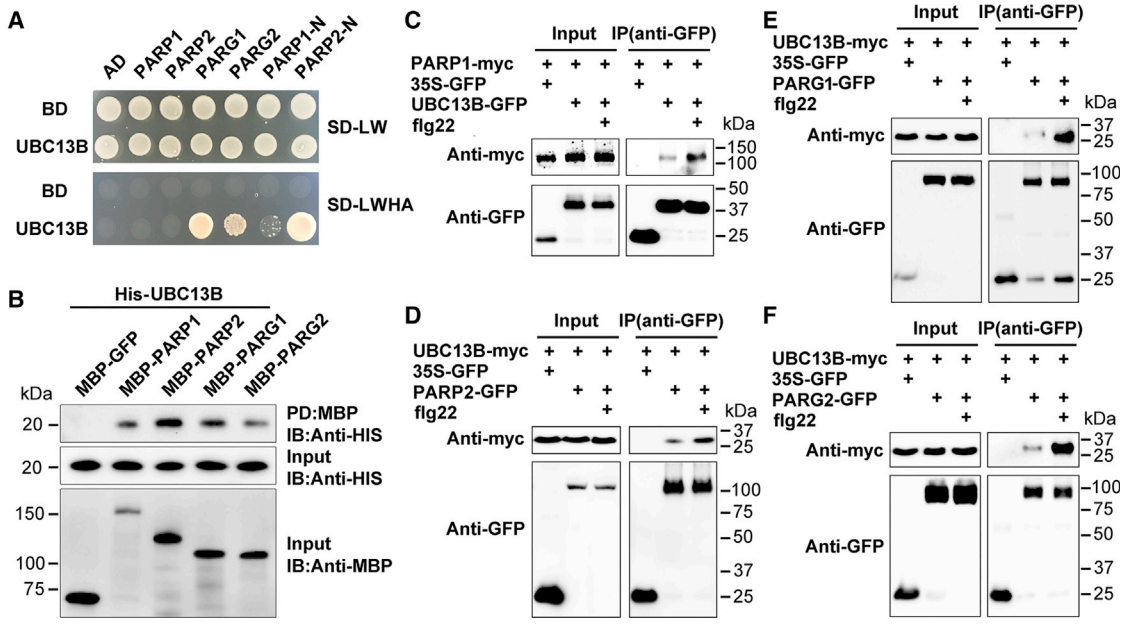

Figure 1. UBC13B directly interacts with PARP1, PARP2, PARG1, and PARG2.

(A) UBC13B interacts with PARP1, PARP2, PARG1, and PARG2 in yeast. Equal amounts of yeast cells expressing the indicated bait (BD, pGBKT7) and prey (AD, pGADT7) constructs were grown on SD-Leu-Trp (SD-LW) and SD-Leu-Trp-His-Ade (SD-LWHA) plates. Three independent experiments were carried out with similar results.

(B) UBC13B interacts with PARP1, PARP2, PARG1, and PARG2 *in vitro*. HIS-tagged UBC13B was incubated with immobilized MBP-tagged GFP, PARP1, PARP2, PARG1, or PARG2 proteins. The input samples and immunoprecipitated fractions were detected by anti-HIS or anti-MBP antibody. Two independent experiments were carried out with similar results.

(C–F) UBC13B interacts with PARP1, PARP2, PARG1, PARG2 *in vivo*. UBC13B-GFP was coexpressed with PARP1-myc in *N. benthamiana*. UBC13B-myc was coexpressed with GFP-tagged PARP2, PARG1, or PARG2 in *N. benthamiana*. All constructs were driven by the 35S promoter. Total proteins were extracted, immunoprecipitated with GFP-Trap magnetic beads, and immunoblotted with anti-myc or anti-GFP antibody. Plants were treated without or with 1 μM flg22 for 1 h. Three independent experiments were carried out with similar results.

using a chemical proteomic approach, respectively (Gibson et al., 2016). To confirm the interaction and investigate whether Arabidopsis UBC13B associates with other PARP and PARG proteins, we carried out a yeast two-hybrid assay. As shown in Figure 1A, in addition to PARG2, UBC13B also interacts with the full-length PARG1 and the N-terminal region of PARP2. To further validate the physical interactions of UBC13B with these proteins, we performed *in vitro* pull-down assays. MBP-tagged PARP1, PARP2, PARG1, or PARG2 could pull down HIS-tagged UBC13B (Figure 1B). Next, we determined whether UBC13B interacts with PARPs and PARGs *in vivo*. Co-immunoprecipitation (co-IP) assays revealed that UBC13B was detected in the precipitates of PARP1, PARP2, PARG1, and PARG2, and these interactions were enhanced by flg22 treatment (Figure 1C–1F). Similarly, we found that UBC13A, the highly homologous protein of UBC13B, also associates with PARP1, PARP2, PARG1, and PARG2, and flg22 treatment facilitates their interactions (Supplemental Figure 1). These data indicate that the E2 ubiquitin-conjugating enzyme UBC13 physically interacts with PARP1, PARP2, PARG1, and PARG2, and PAMP treatment promotes their interactions.

UBC13 is involved in plant immunity

To investigate the role of *UBC13* in plant immunity, we obtained one T-DNA insertion line WiscDsLox323H12 (*ubc13a-1*) for *UBC13A* and two independent insertion lines for *UBC13B*: SALK_047381 (*ubc13b-1*) and GABI_836B11 (*ubc13b-2*) (Supplemental Figure 2A). qRT-PCR assays showed that the transcripts of *UBC13A* in *ubc13a-1* and *UBC13B* in *ubc13b-2* were absent (Figure 2A), indicating that both mutants are null. However, the transcript of *UBC13B* in *ubc13b-1* was still detected at a low level (Figure 2A), in agreement with a previous report (Li and Schmidt, 2010). An anti-human UBC13 monoclonal antibody 4E11 was shown to be able to detect the UBC13 proteins in Arabidopsis (Andersen et al., 2005). Western blot analysis indicated that the accumulation of UBC13 proteins was slightly compromised in *ubc13a-1* but dramatically decreased in *ubc13b-2* compared with that of wild-type (WT) plants. A longer exposure showed that the UBC13 proteins were still detected in the *ubc13a-1 ubc13b-1* double mutant but not in the *ubc13a-1 ubc13b-2* mutant (Figure 2B), confirming again that the *ubc13a-1 ubc13b-2* mutant is null. Therefore, the *ubc13a-1 ubc13b-2* double mutant was selected for the rest of the studies and was herein referred to as *ubc13a ubc13b*.

None of the single mutants showed any visible phenotypes compared with WT plants. The *ubc13a ubc13b* double mutant exhibited severe growth and developmental defects, including dwarf stature, short roots, and yellow leaves, which are consistent with previous results (Figure 2C and Supplemental Figure 2B and 2C) (Romero-Barrios et al., 2020). The *ubc13a ubc13b* mutant plants only produced a few shrunken seeds that were unable to germinate (Supplemental Figure 2D).

Please cite this article in press as: Yao et al., Coordinated regulation of plant immunity by poly(ADP-ribosyl)ation and K63-linked ubiquitination, Molecular Plant (2021), https://doi.org/10.1016/j.molp.2021.08.013

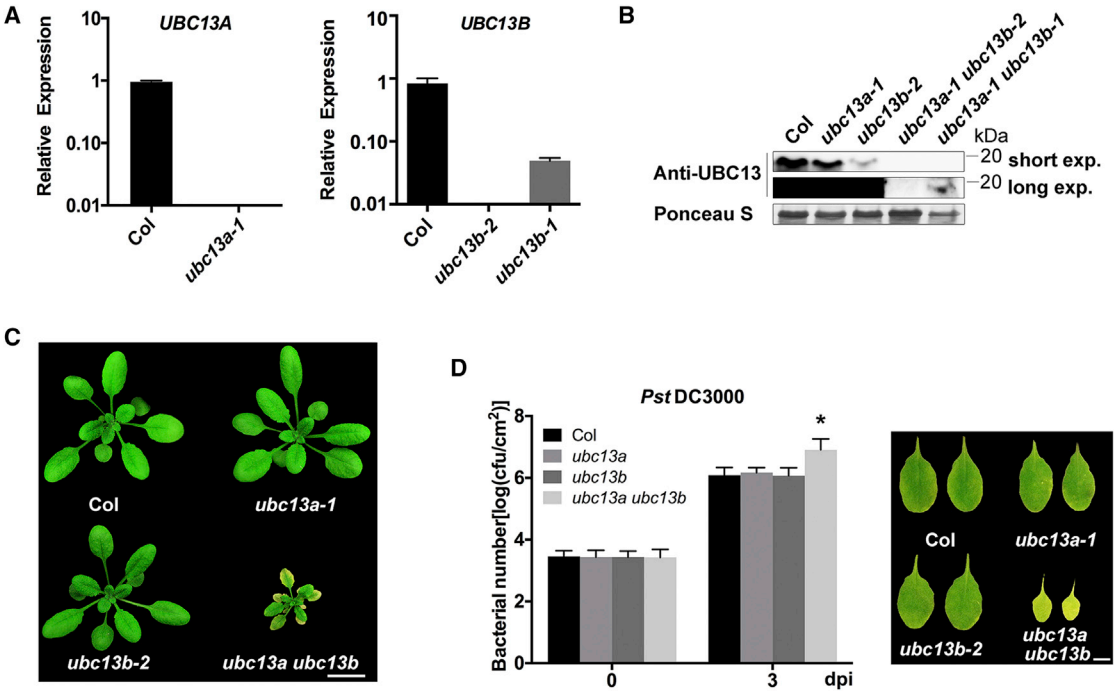

Figure 2. UBC13 is required for plant immunity.

(A) qRT-PCR expression analysis of Arabidopsis *UBC13A* and *UBC13B* in WT Col, *ubc13a-1*, *ubc13b-1*, and *ubc13b-2*. Data are shown as the mean ± SD (n =3). Three independent experiments were carried out with similar results.

(B) The accumulation of UBC13 protein in *ubc13a-1*, *ubc13b-2*, *ubc13a-1 ubc13b-2*, and *ubc13a-1 ubc13b-1* mutants. Total proteins were extracted from 3-week-old plants, separated on SDS-PAGE, immunoblotted with anti-UBC13 antibody. Short and long exposures of the immunoblot are shown. Equal loading was confirmed by Ponceau S staining. Three independent experiments were carried out with similar results.

(C) The growth phenotype of 3-week-old *ubc13a-1*, *ubc13b-2*, and *ubc13a ubc13b* mutants. Scale bar, 1 cm.

(D) The *ubc13a ubc13b* double mutant is more susceptible to *Pst* DC3000. Leaves of 3-week-old plants were inoculated with *Pst* DC3000 at an OD_{600} of 0.0005. Bacterial numbers were determined at 0 and 3 days postinoculation (dpi). Data are shown as the mean ± SD (n = 8). Three independent experiments were carried out with similar results. The asterisk indicates a significant difference from Col (analysis of variance [ANOVA], Tukey's pairwise comparisons, $^*P < 0.05$). Leaf pictures were taken at 3 dpi. Scale bar, 1 cm.

To determine whether UBC13 is involved in plant immunity, the *ubc13a-1*, *ubc13b-2*, and *ubc13a ubc13b* mutants were infected with the bacterial pathogen *Pst* DC3000. As shown in Figure 2D, the *ubc13a-1* or *ubc13b-2* single mutant showed a similar level of resistance to *Pst* DC3000 compared with WT plants, whereas the *ubc13a ubc13b* double mutant exhibited enhanced susceptibility to *Pst* DC3000 (Figure 2D), which is in line with a previous study using the weak *ubc13a-1 ubc13b-1* allele (Turek et al., 2018).

PARylation of UBC13 is induced by Flg22 treatment and promotes its association with PARP2

The physical interaction of UBC13 with PARP1/2 and PARG1/2 suggests that UBC13 is potentially PARylated. To determine whether UBC13 is a PARP target, we performed *in vitro* PARylation assays and found that UBC13B was robustly PARylated by PARP2 (Figure 3A). To confirm whether UBC13B is PARylated *in vivo*, we expressed GFP-tagged UBC13B in *Nicotiana benthamiana*. The UBC13B fusion proteins were immunoprecipitated with anti-GFP antibody and subjected to western blot analysis. A distinct band was detected from the immunoprecipitates with an anti-pan-ADPR reagent and was considerably increased upon flg22 treatment (Figure 3B). Taken together, these results demonstrate that UBC13B is PARylated by PARP2 and PARylation of UBC13B is enhanced by PAMP treatment.

To identify PARylation residues of UBC13B by PARP2, we took a site-specific proteomic approach by LC-MS/MS (Feng et al., 2016; Zhang et al., 2013) and found that five glutamic acid residues on the N-terminus of UBC13B were PARylated, some of which are next to each other (E40/E41, E71/E72, Figure 3C and 3D, Supplemental Figure 3, and Supplemental Table 1). Two consecutive glutamic acid residues (EE) are conserved sites that often serve for protein PARylation (Le May et al., 2012). To verify that these residues are PARylated, we mutated glutamic acid to alanine to produce $UBC13B^{2E1}$ (E40/E41), $UBC13B^{2E2}$ (E71/72), $UBC13B^{4E}$ (E40/E41/E71/72), and $UBC13B^{8E}$ with all eight glutamic acid residues substituted with alanine on the N-terminus of UBC13B. As expected, *in vitro* PARylation assays showed that WT UBC13B was robustly PARylated by PARP2, whereas both $UBC13B^{2E1}$ and $UBC13B^{2E2}$ mutants were PARylated to a lesser extent (Figure 3E). Furthermore, mutations with combinations of these quadruple sites ($UBC13B^{4E}$) together with additional alanine substitutions ($UBC13B^{8E}$) displayed no detectable PARylation (Figure 3E). These results indicate that the quadruple E40/E41/E71/E72 residues are the primary PARylation sites of UBC13B.

We next examined the effect of the quadruple mutations of UBC13B on its interaction with PARP2. Co-IP assays showed

Please cite this article in press as: Yao et al., Coordinated regulation of plant immunity by poly(ADP-ribosyl)ation and K63-linked ubiquitination, Molecular Plant (2021), https://doi.org/10.1016/j.molp.2021.08.013

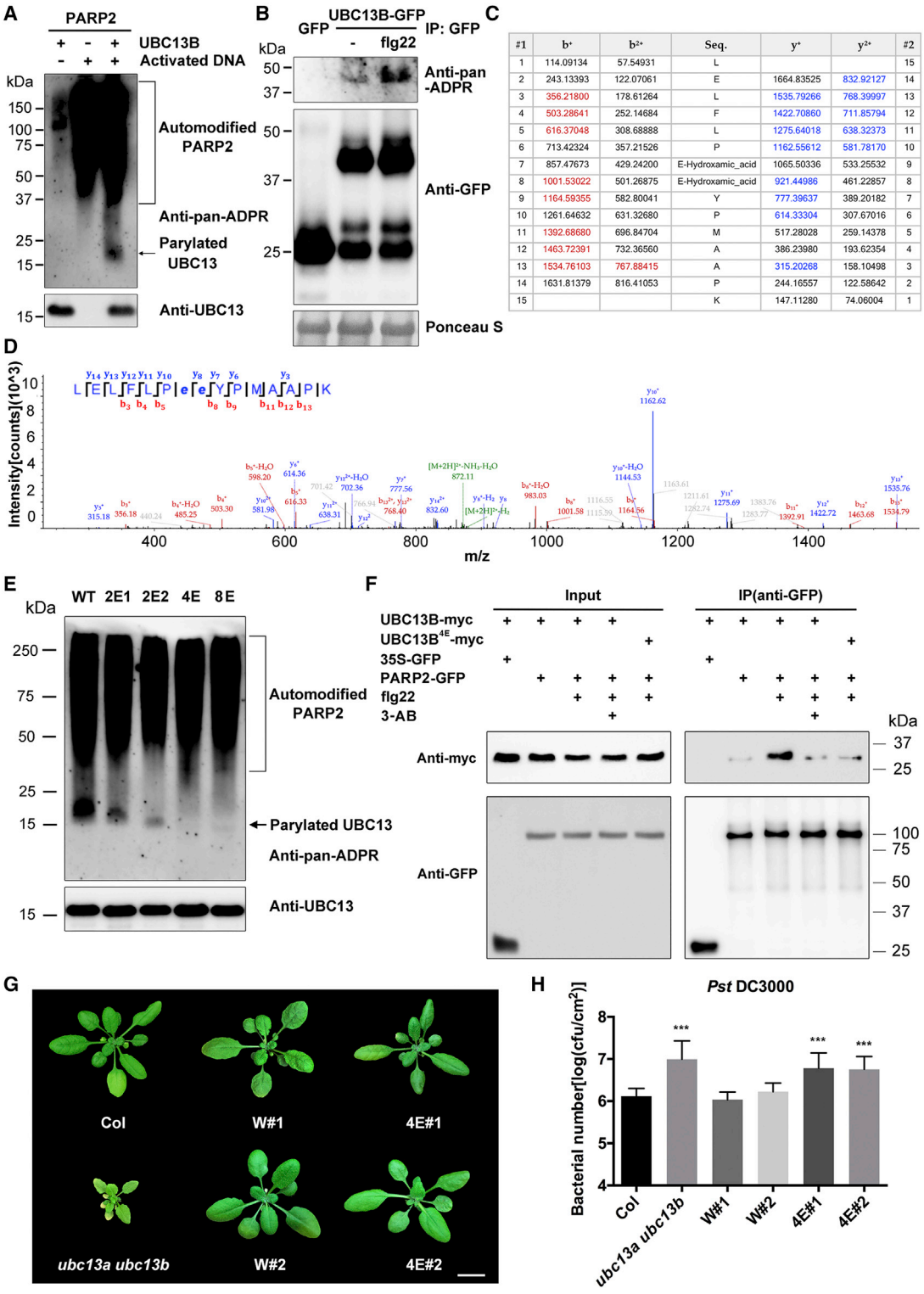

#1	b+	b2+	Seq.	y+	y2+	#2
1	114.09134	57.54931	L			15
2	243.13393	122.07061	E	1664.83525	832.92127	14
3	356.21800	178.61264	L	1535.79266	768.39997	13
4	503.28641	252.14684	F	1422.70860	711.85794	12
5	616.37048	308.68888	L	1275.64018	638.32373	11
6	713.42324	357.21526	P	1162.55612	581.78170	10
7	857.47673	429.24200	E-Hydroxamic_acid	1065.50336	533.25532	9
8	1001.53022	501.26875	E-Hydroxamic_acid	921.44986	461.22857	8
9	1164.59355	582.80041	Y	777.39637	389.20182	7
10	1261.64632	631.32680	P	614.33304	307.67016	6
11	1392.68680	696.84704	M	517.28028	259.14378	5
12	1463.72391	732.36560	A	386.23980	193.62354	4
13	1534.76103	767.88415	A	315.20268	158.10498	3
14	1631.81379	816.41053	P	244.16557	122.58642	2
15			K	147.11280	74.06004	1

Figure 3. Identification of PARylation sites in UBC13B.

(A) *In vitro* PARylation of UBC13B by PARP2. An equal amount of purified recombinant MBP-PARP2 protein was incubated with or without HIS-UBC13B and activated DNA in a PARylation reaction. PARylated proteins were detected with an anti-pan-ADPR reagent. Three independent experiments were carried out with similar results.

(B) Flg22 induces UBC13B PARylation *in vivo*. The UBC13B-GFP construct under the control of the 35S promoter was expressed in *N. benthamiana* and samples were collected 1 h after treatment with 1 μM flg22. UBC13B-GFP was immunoprecipitated with GFP-Trap magnetic beads and the PARylated proteins were detected with an anti-pan-ADPR reagent. Three independent experiments were carried out with similar results.

(legend continued on next page)

Please cite this article in press as: Yao et al., Coordinated regulation of plant immunity by poly(ADP-ribosyl)ation and K63-linked ubiquitination, Molecular Plant (2021), https://doi.org/10.1016/j.molp.2021.08.013

that the interaction of WT UBC13B with PARP2 was enhanced by flg22 treatment. In contrast, the quadruple mutant UBC13B^{4E} exhibited significantly reduced binding affinity to PARP2 in response to flg22 (Figure 3F). This is consistent with the finding that flg22-induced UBC13B-PARP2 association was markedly suppressed by 3-aminobenzamide (3-AB), a broad PARP inhibitor (Figure 3F). These results suggest that PARylation promotes the association of UBC13B with PARP2.

PARylation of UBC13 is required for plant immunity

To further reveal the biological functions of UBC13 PARylation in growth, development, and immunity, we transformed WT *UBC13B* and its *UBC13B*^{4E} mutant under the control of its native promoter into the *UBC13A ubc13a/ubc13b ubc13b* heterozygous mutant background. The resulting transgenic lines were selfed, and homozygous *ubc13a* lines were identified. The expression of UBC13B-myc was confirmed by immunoblotting using an anti-UBC13 or an anti-myc antibody (Supplemental Figure 4). Two independent stable lines were selected for further analysis. The transgenic lines carrying the *UBC13B*^{4E} mutant showed normal morphology and were phenotypically indistinguishable from the lines expressing WT *UBC13B*, suggesting that both *UBC13B* and *UBC13B*^{4E} can complement the developmental defects of the *ubc13a ubc13b* double mutant (Figure 3G). We next examined whether the *UBC13B* and *UBC13B*^{4E} transgenic lines respond similarly to pathogens. As shown in Figure 3H, the *UBC13B* transgene completely restored disease resistance of the *ubc13a ubc13b* mutant to *Pst* DC3000, but the *UBC13B*^{4E} transgenic plants were still susceptible to bacterial infection at a similar level to *ubc13a ubc13b* (Figure 3H). These results indicate that PARylation of UBC13 contributes to its function in plant immunity.

PTI responses are altered in *parp* and *ubc13* mutants

To elucidate the underlying mechanism of the compromised immune response in *parp* and *ubc13a ubc13b* mutants, we examined the transcript levels of defense marker genes, MAPK activities, callose deposition, and ROS burst in the *parp* and *ubc13a ubc13b* mutants. In the resting state, the *ubc13a ubc13b* mutant showed a high level of basal *PR1* gene expression (Figure 4A). At 12 h and 24 h after flg22 treatment, the *parp2*, *parp1 parp2*, and *ubc13a ubc13b* mutants displayed markedly increased *PR1* expression compared with WT and *parp1* mutant plants (Figure 4A). For early defense marker genes, the expression of *WRKY30* was increased in the *parp2*, *parp1 parp2*, and *ubc13a ubc13b* mutants upon flg22 treatment, whereas the expression of *FRK1* was only increased in the *ubc13a ubc13b* double mutant but not in the *parp1*, *parp2*, and *parp1 parp2* mutants. For the other two marker genes AT1G07160 and AT2G17740, no noticeable changes were observed in any of the *parp* and *ubc13a ubc13b* mutants (Figure 4B). A MAPK assay showed that flg22 treatment elicited a stronger activation of MPK3 and MPK6 in *parp2*, *parp1 parp2*, and *ubc13a ubc13b* mutants compared with WT and *parp1* mutant plants (Figure 4C). Callose deposition is a late response during PAMP-triggered immunity. No altered callose deposition was observed in the single and double *ubc13* mutants compared with WT plants upon flg22 treatment (Supplemental Figure 5A and 5B). No significant difference in the flg22-induced ROS burst was observed for the single and double *parp* mutants; however, the flg22-triggered ROS burst was impaired in the *ubc13a ubc13b* mutant (Supplemental Figure 5C). We next examined flg22-induced PTI responses in the *UBC13B*^{4E} lines. As shown in Supplemental Figure 6, *UBC13B*^{4E} failed to complement the heightened expression of *PR1* and *WRKY30* and increased activation of MPK3 and MPK6 in *ubc13a ubc13b* in response to flg22, suggesting that PARylation of UBC13 contributes to PTI.

Secretion of PR1 is compromised in *parp* and *ubc13a ubc13b* mutants

The central immune regulator NPR1 controls the expression of protein secretory pathway genes, and disruption of these components resulted in defective secretion of PR proteins and compromised defense responses (Wang et al., 2005). Notably, the PAMP elicitor flg22 also induces systemic acquired resistance (SAR) (Mishina and Zeier, 2007) and the expression of ER chaperone genes, including *BIP1/2*, *ERdj3B*, and *SDF2,* whose products complex to cope with the massive demand of endoplasmic reticulum (ER)-associated protein synthesis during PTI (Arrano-Salinas et al., 2018). The impaired immune response to bacterial pathogens in the *parp* and *ubc13a ubc13b* mutants with increased expression of *PR* genes upon flg22 treatment is unexpected (Figure 4A) as the production and secretion of antimicrobial PR proteins is a major defense mechanism against bacterial pathogens. We speculated that secretion of PR proteins in the *parp* and *ubc13a ubc13b* mutants might be affected and thus examined the levels of total and extracellular PR1 proteins in the *parp* and *ubc13a*

(C) List of the mass/charge values of b^+ ions and y^+ ions of the peptide (LELFLPEEYPMAAPK). PARylated Glu (E) sites are indicated by E-Hydroxamic_acid. The mass values in red and blue correspond to the identified b^+ ions and y^+ ions peaks in the spectrum.

(D) MS/MS spectrum of a doubly charged peptide with PARylated Glu sites. The "e" in bold and lowercase indicates a modified Glu residue.

(E) The EE mutations in UBC13B substantially diminish its PARylation *in vitro*. An equal amount of purified recombinant HIS-tagged UBC13B, UBC13^{2E1}, UBC13^{2E2}, UBC13^{4E}, or UBC13^{8E} protein was incubated with MBP-PARP2 in a PARylation reaction. PARylated proteins were detected with an anti-pan-ADPR reagent.

(F) The 4E mutation in UBC13B reduces its interaction with PARP2 in response to flg22 *in vivo*. Myc-tagged UBC13B or UBC13B^{4E} under the control of the 35S promoter was coexpressed with PARP2-GFP in *N. benthamiana.* Total proteins were extracted, immunoprecipitated with GFP-Trap magnetic beads, and immunoblotted with anti-myc or anti-GFP antibody. Leaves were treated with 3-AB for 1 day prior to treatment with 1 μM flg22 for 1 h.

(G) Phenotypes of the *ubc13a ubc13b* mutant complemented with WT *UBC13B* or *UBC13B*^{4E}. Three-week-old plants of two independent transgenic lines carrying *ProUBC13B:UBC13B-myc/ubc13a ubc13b* (W#1 and W#2) or *ProUBC13B:UBC13B*^{4E}*-myc/ubc13a ubc13b* (4E#1 and 4E#2) were shown. Scale bar, 1 cm.

(H) The 4E mutation in UBC13B abolishes its resistance to *Pst* DC3000. Three-week-old transgenic plants were inoculated with *Pst* DC3000 at an OD_{600} of 0.0005. Bacterial numbers were determined at 3 days postinoculation (dpi). Data are shown as the mean ± SD (n = 8). Three independent experiments were carried out with similar results. The asterisk indicates a significant difference from Col (analysis of variance [ANOVA], Tukey's pairwise comparisons, ***$P < 0.001$).

Please cite this article in press as: Yao et al., Coordinated regulation of plant immunity by poly(ADP-ribosyl)ation and K63-linked ubiquitination, Molecular Plant (2021), https://doi.org/10.1016/j.molp.2021.08.013

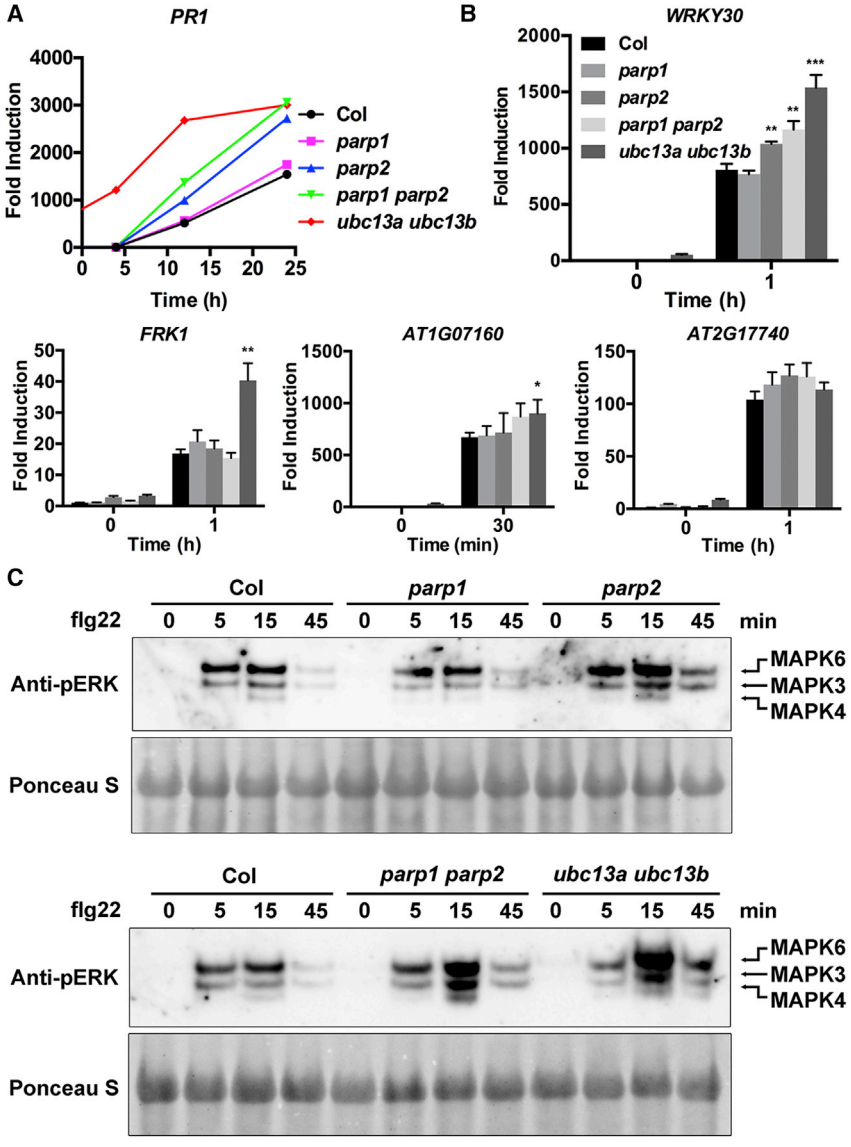

Figure 4. PTI responses in the *parp* and *ubc13* mutants.

(A) Flg22-induced *PR1* transcript level was enhanced in the *parp* and *ubc13* mutants. Ten-day-old Arabidopsis seedlings were treated with 1 μM flg22 for 0, 4, 12, and 24 h. Data are shown as the mean ± SD (n =3). Three independent experiments were carried out with similar results.

(B) Flg22-induced PTI marker gene expression in the *parp* and *ubc13* mutants. Ten-day-old seedlings were treated with 1 μM flg22 for 30 or 60 min for qRT-PCR analysis. Data are shown as the mean ± SD (n = 3). The asterisk indicates a significant difference from Col (analysis of variance [ANOVA], Tukey's pairwise comparisons, $^{*}P < 0.05$, $^{**}P < 0.01$, $^{***}P < 0.001$). Three independent experiments were carried out with similar results.

(C) Flg22-induced MAPK activation in the *parp* and *ubc13* mutants. Ten-day-old seedlings were treated with 1 μM flg22 and collected at 0, 5, 15, and 45 min after treatment. MAPK activation was detected by Western blot with anti-pERK antibody. Equal loading was confirmed by Ponceau S staining. Three independent experiments were carried out with similar results.

ubc13b mutants after *Pst* DC3000 infection. Western blot analysis revealed a moderately enhanced accumulation of total PR1 protein in the *parp2* and *parp1 parp2* mutants and a more pronounced increase in *ubc13a ubc13b* compared with WT (Figure 5A). In contrast, the extracellular PR1 level was clearly reduced in *parp2*, *parp1 parp2*, and *ubc13a ubc13b* compared with WT (Figure 5A), suggesting that secretion of PR1 is compromised in the *parp* and *ubc13a ubc13b* mutants.

We next examined whether the *parp* and *ubc13a ubc13b* mutants can mount an effective immune response against the virulent *Pst* DC3000 after flg22 elicitation. The WT and *parp1* mutant plants pretreated with flg22 showed a significant reduction in pathogen growth compared with mock-treated control plants. In contrast, the *parp2*, *parp1 parp2*, and *ubc13a ubc13b* mutants failed to establish resistance induced by flg22 (Figure 5B). We further evaluated the ability of *parp* and *ubc13a ubc13b* mutants to induce SAR. The *parp1* mutant showed enhanced resistance against *Pst* DC3000 after SA treatment similar to WT. However, SAR was not induced in the *parp2*, *parp1 parp2*, and *ubc13a ubc13b* mutants (Figure 5C).

PDI proteins interact with PARP2 and PARG1

Previous studies have uncovered membrane traffic components, such as SEC61 and SYP132, and ER-resident chaperones and co-chaperones, including BIP2, defender against apoptotic death 1 (DAD1), and PDIs that are essential for proper folding and secretion of PR proteins (Kalde et al., 2007; Wang et al., 2005). Among protein disulfide isomerases, PDIA3, PDIA5, PDIA6, P4HB, and SEC61G were identified as PARP targets in humans by proteomic approaches (Gagne et al., 2012; Gibson et al., 2016; Martello et al., 2016; Westcott et al., 2017). Interestingly, a number of secretory pathway proteins, including BIP2, SYP122, SYP132, PDI1, PDI2, PDI5, and PDI6, were found to putatively undergo K63-linked ubiquitination (Johnson and Vert, 2016; Romero-Barrios et al., 2020). To determine whether these secretory pathway proteins are targeted for PARylation and K63-linked ubiquitination, we first examined their interaction with PARPs, PARGs, and UBC13 by a yeast two-hybrid analysis. As shown in Figure 6A, PDI2 was found to interact with PARG1. PDIs are a family of ubiquitous proteins that are localized in the ER, nucleus, chloroplast, and other cellular compartments (Cho et al., 2011; Kleffmann et al., 2004; Wittenberg et al., 2014). They catalyze the formation, reduction, and isomerization of disulfide bonds between cysteine residues to facilitate the maturation of nascent secretory proteins and ensure proper folding and assembly of proteins (Feige and Hendershot, 2011; Gruber et al., 2006). Notably, flg22 treatment results in an

Please cite this article in press as: Yao et al., Coordinated regulation of plant immunity by poly(ADP-ribosyl)ation and K63-linked ubiquitination, Molecular Plant (2021), https://doi.org/10.1016/j.molp.2021.08.013

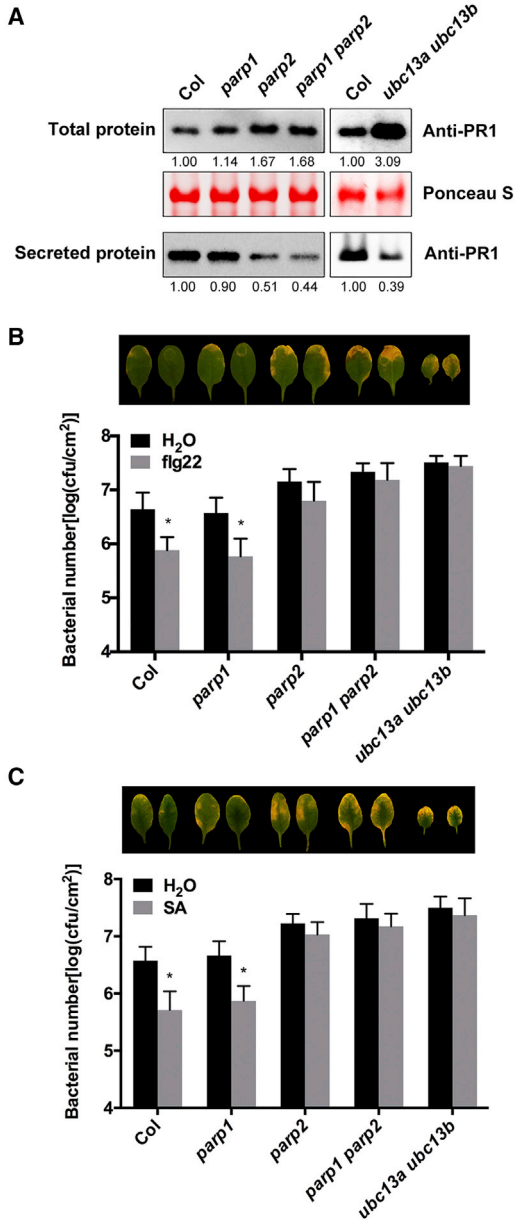

Figure 5. Effects of *parp* and *ubc13* mutations on PR1 secretion and resistance against *Pst* DC3000.

(A) The accumulation of total and secreted PR1 proteins in the *parp* and *ubc13* mutants. Total and secreted proteins were prepared from 3-week-old plants infiltrated with *Pst* DC3000 at an OD_{600} of 0.02, separated on SDS-PAGE, and immunoblotted with anti-PR1 antibody. The band intensities were determined by ImageJ and normalized to that of WT. Equal loading was confirmed by Ponceau S staining. Experiments were repeated three times with similar results.

(B) Flg22-induced resistance is compromised in the *parp* and *ubc13* mutants. Three-week-old plants were treated with 1 μM flg22 for 4 h prior to inoculation with *Pst* DC3000 at an OD_{600} of 0.001. Bacterial numbers were determined at 3 days postinoculation (dpi), with the initial *Pst* DC3000 inoculum of OD_{600} = 0.001. Data are shown as the mean ± SD (n = 8). Three independent experiments were carried out with similar results. The asterisk indicates a significant difference between H_2O and flg22 pretreated samples (analysis of variance [ANOVA], Tukey pairwise comparisons, $^*P < 0.05$). Leaf pictures were taken at 3 dpi.

(C) SA-induced resistance is compromised in the *parp* and *ubc13* mutants. Three-week-old plants were pretreated with 1 mM SA for 24 h prior to inoculation with *Pst* DC3000 at an OD_{600} of 0.001. Bacterial numbers were determined at 3 dpi. Data are shown as the mean ± SD (n = 8). Three independent experiments were carried out with similar results. The asterisk indicates a significant difference between H_2O and SA pretreated samples (analysis of variance [ANOVA], Tukey's pairwise comparisons, $^*P < 0.05$). Leaf pictures were taken at 3 dpi.

alteration of cellular redox homeostasis and an increased accumulation of PDI proteins (Balmant, 2016; Wang et al., 2012). It is known that some PDI family members in humans (Koivunen et al., 1999; Lucero and Kaminer, 1999) and four PDI proteins in Arabidopsis, PDI1, PDI2, PDI3, and PDI4 (Yuen et al., 2013), appear to be enriched for acidic glutamic and aspartic residues, which are two preferred ADP-ribosylation acceptor sites (D'Amours et al., 1999; Hassa et al., 2006), suggesting that PDIs are potential PARP targets. Therefore, we examined whether other Arabidopsis PDIs interact with PARPs, PARGs, and UBC13 proteins. The Arabidopsis genome encodes 12 PDI proteins, among which PDI3, PDI4, PDI7, and PDI12 are expressed at a low level (Lu and Christopher, 2008). We cloned the cDNAs of 11 Arabidopsis *PDI* genes except for *PDI12* and examined their interaction with PARG1. Yeast two-hybrid analysis showed that, in addition to PDI2, PDI3 also interacts with PARG1; however, PDI1, PDI4, PDI9, and PDI10 have strong autoactivation activities despite the addition of 20 mM 3-amino-1,2,4-triazole (3-AT) (Figure 6B). To further confirm the physical interactions of PDIs with PARG1 and PARP2, we performed *in vitro* pull-down assays. MBP-tagged PDI1, PDI2, PDI3, or PDI4 could pull-down HIS-tagged PARG1 or PARP2 (Supplemental Figure 7A and 7B). Next, we investigated whether PDI1, PDI2, PDI3, and PDI4 interact with PARG1 *in vivo*. Co-IP revealed that all four PDI proteins associate with PARG1 and their interactions are enhanced by flg22 treatment (Figure 6C–6F). Furthermore, the four PDIs also complex with PARP2 *in vivo*, and these associations are enhanced by flg22 treatment (Supplemental Figure 7C–7F). In addition, we performed a co-IP assay of the interaction between PARG1 and PDI1 using Arabidopsis mesophyll protoplasts and confirmed that their interaction also occurs in Arabidopsis (Supplemental Figure 8). The undetectable interaction of PDIs with PARPs in yeast is not unexpected, as it was similarly observed between PARP1 and a DNA binding protein aprataxin in humans (Date et al., 2004), likely due to incorrect folding or a requirement of posttranslational modifications that are absent in yeast.

PARylation of PDIs facilitates their K63 ubiquitination and contributes to disulfide isomerase activities

The association of PDIs with PARP2 and PARG1 suggests that PDIs may be PARylated. To test whether PDIs are PARylated *in vivo*, we focused on two PDIs, PDI1 and PDI3, and overexpressed them in *N. benthamiana*. GFP-tagged PDI proteins were enriched by immunoprecipitation with anti-GFP antibody followed by immunoblotting with an anti-pan-ADPR reagent. In the absence of induction, no obvious PARylation activity of PDI1 and PDI3 was detected. Upon flg22 treatment, profound PARylation of PDI1 and PDI3 was observed, whereas addition of the PARP inhibitor 3-AB together with flg22 led to marked reduction of PARylation, indicating that PDI1 and PDI3 are PARylated in a flg22-dependent manner (Figure 7A). To further demonstrate that PDI proteins are PARylated, we took a

Please cite this article in press as: Yao et al., Coordinated regulation of plant immunity by poly(ADP-ribosyl)ation and K63-linked ubiquitination, Molecular Plant (2021), https://doi.org/10.1016/j.molp.2021.08.013

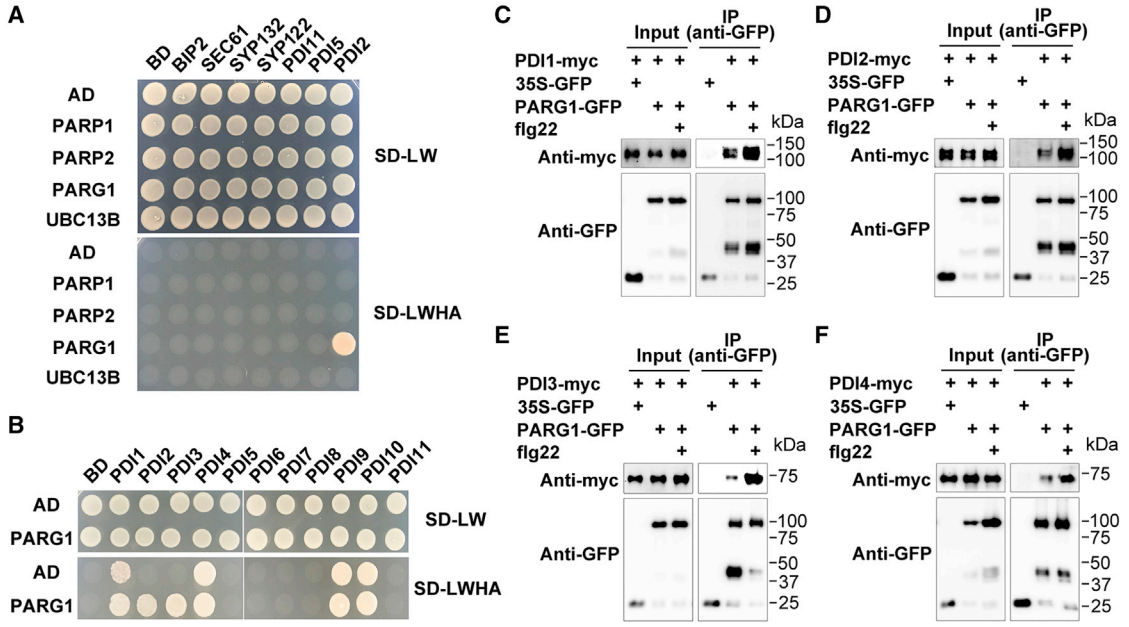

Figure 6. PDIs interact with PARG1.

(A) PDI2 interacts with PARG1 in yeast. pGBKT7 (BD) and pGADT7 (AD) empty vectors were used as negative controls. Equal amounts of cells were spotted on SD-LW and SD-LWHA plates. Three independent experiments were carried out with similar results.

(B) Yeast two-hybrid analysis of interactions of PDIs with PARG1. Equal amounts of cells were spotted on SD-LW and SD-LWHA plates containing 20 mM 3-AT. Three independent experiments were carried out with similar results.

(C–F) PDI1, PDI2, PDI3, and PDI4 interact with PARG1 *in vivo*. PARG1-GFP was coexpressed with myc-tagged PDI1, PDI2, PDI3, and PDI4 in *N. benthamiana*. All constructs were driven by the 35S promoter. Total proteins were extracted, immunoprecipitated with GFP-Trap magnetic beads, and immunoblotted with anti-myc or anti-GFP antibody. Plants were treated without or with 1 μM flg22 for 1 h. Three independent experiments were carried out with similar results.

site-specific proteomic approach to identify PARylation sites in PDI1, PDI2, PDI3, and PDI4. Mass spectrometry results showed that four, four, and five Glu or Asp residues from PDI1, PDI3, and PDI4, respectively, are PARylated by PARP2 (Supplemental Table 2). However, no PARylation sites were identified in PDI2, possibly due to the low abundance of PARylation or the presence of PARylation sites other than Glu and Asp.

The findings that UBC13 associates with and is PARylated by PARP proteins indicate that K63-linked ubiquitination may be regulated by PARylation. To elucidate the mechanistic link between the two posttranslational modifications, we monitored the K63-linked ubiquitination levels in WT and *parp* mutants. As shown in Figure 7B and 7C, the accumulation of K63-linked ubiquitination was significantly induced in WT plants after flg22 treatment. The *parp1* single mutant displayed a similar level of K63-linked ubiquitination compared with WT. However, the K63-linked ubiquitination abundance was greatly diminished in the *parp2* and *parp1 parp2* mutants, suggesting that K63-linked ubiquitination is dependent on PARylation primarily mediated by PARP2. Numerous PDI proteins were shown to be putatively ubiquitinated at K63 (Johnson and Vert, 2016; Romero-Barrios et al., 2020). To verify whether PDI proteins are K63 ubiquitinated, we expressed two PDI proteins, PDI1 and PDI3, which were shown to be PARylated (Figure 7A), in *N. benthamiana* and performed immunoprecipitation. The PDI precipitates were probed with the K63-linkage specific ubiquitination antibody. Immunoblotting revealed that both PDI1 and PDI3 undergo K63-linked ubiquitination upon flg22 treatment. To further elucidate the relationship between PARylation and K63-linked ubiquitination, we treated the PDI-expressing plants with 3-AB 24 h prior to flg22 treatment. Intriguingly, inhibition of PARylation by 3-AB blocked flg22-dependent K63-linked ubiquitination (Figure 7A), suggesting that PARylation contributes to K63-linked ubiquitination.

To examine whether PARylation and K63-linked ubiquitination are involved in PDI function, we measured the overall disulfide isomerase activity in the leaves of WT, *parp1 parp2*, and *ubc13a ubc13b* plants. As shown in Figure 7D, protein disulfide isomerase activity was lower in the *parp1 parp2* and *ubc13a ubc13b* mutants than in the WT control. These results indicate that both PARylation and K63-linked ubiquitination contribute to the protein disulfide isomerase activity. We also analyzed the PDI activity of the *pdi1* mutant. As shown in Supplemental Figure 9, the *pdi1* mutant showed a similar level of PDI activity compared with WT, likely due to functional redundancy of the 12 *PDI* genes encoded by the Arabidopsis genome.

As evolutionarily conserved molecular chaperones in eukaryotes, PDIs are known to play an essential role in a surveillance mechanism termed endoplasmic reticulum quality control (ERQC), which ensures that only properly folded proteins are delivered to their final destination (Strasser, 2018). Accumulation of misfolded or unfolded proteins beyond the capacity of the ERQC system activates the unfolded protein response (UPR) (Liu and Howell, 2010; Saijo, 2010). To investigate whether the ERQC pathway is affected in the *parp* and *ubc13* mutants, we examined the expression of *BIP* genes, whose products are

Please cite this article in press as: Yao et al., Coordinated regulation of plant immunity by poly(ADP-ribosyl)ation and K63-linked ubiquitination, Molecular Plant (2021), https://doi.org/10.1016/j.molp.2021.08.013

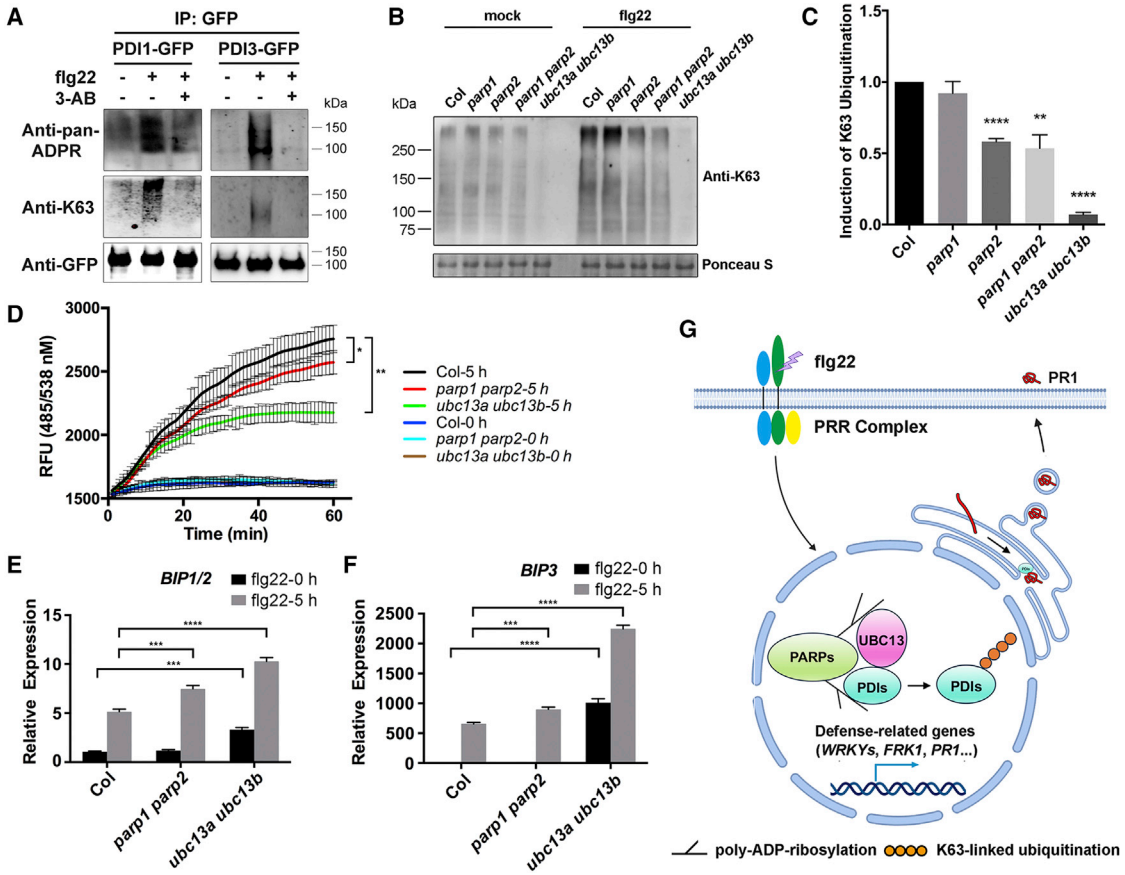

Figure 7. PARylation and K63-linked ubiquitination contribute to protein disulfide isomerase activities.

(A) Flg22 induces PARylation of PDIs and the PARylation enhances K63-linked ubiquitination of PDIs *in vivo*. GFP-tagged PDI1 or PDI3 was expressed in *N. benthamiana* and total proteins were extracted, followed by immunoprecipitation with GFP-Trap magnetic beads. PARylated proteins were detected with an anti-pan-ADPR reagent and K63-linked ubiquitinated proteins were detected with K63-linkage specific antibody. Leaves were treated with 3-AB for 1 day prior to treatment with 1 μM flg22 for 1 h. Three independent experiments were carried out with similar results.

(B) Flg22-induced K63-linked ubiquitination is reduced in the *parp* and *ubc13* mutants. Ten-day-old seedlings was treated with 1 μM flg22 or mock (H_2O) for 6 h. K63-linked ubiquitinated proteins were detected with K63-linkage specific antibody. Equal loading was confirmed by Ponceau S staining. Three independent experiments were carried out with similar results.

(C) Quantification of flg22-induced K63-linked ubiquitination levels in (B). Band intensities were quantified using ImageJ. Data are shown as the mean ± SD from three independent biological experiments. Asterisk indicates a significant difference from Col (ANOVA, Tukey's pairwise comparisons, $^{**}P < 0.01$, $^{****}P < 0.0001$).

(D) PDI activity is reduced in the *parp* and *ubc13* mutants. Ten-day-old seedlings of the *parp* and *ubc13* mutants were treated with or without 10 mM DTT for 5 h and were subjected to protein disulfide isomerase assays. Data are shown as the mean ± SD of three biological replicates. The asterisk indicates a significant difference from Col-5h (analysis of variance [ANOVA], Tukey's pairwise comparisons, $^{*}P < 0.05$, $^{**}P < 0.01$).

(E) Flg22-induced *BIP1/2* expression in the *parp* and *ubc13* mutants. Ten-day-old seedlings were treated with 1 μM flg22 for 5 h and subjected to qRT-PCR. Data are shown as the mean ± SD (n =3). The asterisk indicates a significant difference from Col (analysis of variance [ANOVA], Tukey's pairwise comparisons, $^{***}P < 0.001$, $^{****}P < 0.0001$). Three independent experiments were carried out with similar results.

(F) Flg22-induced *BIP3* expression in the *parp* and *ubc13* mutants. Ten-day-old seedlings were treated with 1 μM flg22 for 5 h and subjected to qRT-PCR. Data are shown as the mean ± SD (n =3). The asterisk indicates a significant difference from Col (analysis of variance [ANOVA], Tukey's pairwise comparisons, $^{***}P < 0.001$, $^{****}P < 0.0001$). Three independent experiments were carried out with similar results.

(G) A proposed model for coordinated regulation of secretory pathway by PARylation and K63-linked ubiquitination. In response to PAMPs or pathogens, PARP proteins are activated and PARylated. Activated PARPs recruit UBC13 and PDIs through physical interaction and PARylation, which in turn facilitates K63-linked ubiquitination of PDIs mediated by UBC13 to activate PDIs. Subsequently, the activated PDIs act cooperatively with other secretory proteins to ensure proper protein folding and secretion of PR proteins into the extracellular space.

essential ERQC components involved in protein synthesis, folding, assembly, and translocation across the ER. In the absence of induction, the *ubc13a ubc13b* mutant showed high levels of basal expression of the *BIP1*, *BIP2*, and *BIP3* genes. In response to flg22, both the *parp1 parp2* and *ubc13a ubc13b* mutants exhibited increased expression of *BIP1*, *BIP2*, and *BIP3* compared with WT (Figure 7E and 7F). These data suggest that the ER stress responses are activated in the *parp* and *ubc13 ubc13b* mutants.

DISCUSSION

In this study, we uncovered a cooperative interplay between PARylation and K63-linked ubiquitination in plant immunity. Our

Please cite this article in press as: Yao et al., Coordinated regulation of plant immunity by poly(ADP-ribosyl)ation and K63-linked ubiquitination, Molecular Plant (2021), https://doi.org/10.1016/j.molp.2021.08.013

genetic and biochemical studies described herein provide a mechanistic basis for the intrinsic connection of the two post-translational modifications. Specifically, we demonstrate that UBC13, the major E2 ubiquitin ligase responsible for the formation of K63-linked polyubiquitin chains, physically interacts with PARPs and PARGs and is PARylated upon PAMP induction. PDIs are both PARylated and K63-linked ubiquitinated in a PAMP-dependent manner. Activation of PDIs may require K63-linked ubiquitination, which is promoted by PAMP-induced PARylation mediated by PARPs. Collectively, our results indicate that PAR-dependent K63-linked ubiquitination may likely serve as a regulatory mechanism to modulate the activity and function of certain PARP target proteins.

The emerging aspect of PARP biology is the functional interplay between ADP-ribosylation and other types of post-translational modifications, such as sumoylation, phosphorylation, and ubiquitination (Pellegrino and Altmeyer, 2016; Gupte et al., 2017; Li et al., 2018). In the DNA damage-induced nuclear factor-κB pathway, PARP1 detects DNA strand breaks and catalyzes PARylation of itself and other substrates. Following activation and dissociation from damage sites, automodified PARP1 assembles a PAR-dependent signalosome, which enables PIASy to sumoylate and activate IKKγ (Stilmann et al., 2009). PARP1 can also recruit ataxia telangiectasia mutated (ATM), a protein kinase activated by DNA double-strand breaks, which in turn phosphorylates IKKγ at Ser85 (Hinz et al., 2010). PARylation-dependent ubiquitination has been identified as a regulatory mechanism to control the stability and degradation of PARP targets by the proteasome. RNF146, a RING-domain E3 ubiquitin ligase, has been shown to bind PAR through its PARP-binding WWE motif. This allows RNF146 to recognize PARylated or PAR-binding proteins and mediate their ubiquitylation for proteasomal degradation (Zhang et al., 2011b; Kang et al., 2011). Similarly, the E3 ligase UHRF1 interacts with PARP1 and promotes ubiquitylation and degradation of a DNA methyltransferase 1 (DNMT1) to regulate heterochromatin-associated events (De Vos et al., 2014). A recent study showed that tankyrase, a human PARP family member, directly catalyzes PARylation on c-Jun N-terminal kinase (JNK), a mitogen-activated protein kinase that induces K63-linked ubiquitination of JNK to promote its kinase activity and physiological function (Li et al., 2018). Here we explored the mechanistic relationship between PARylation and K63-linked ubiquitination. We found that the major driver of K63-linked ubiquitination, UBC13, directly interacts with PARP1, PARP2, PARG1, and PARG2, the main components in PARylation pathway in Arabidopsis, *in vitro* and *in vivo*. In addition, UBC13 is PARylated, and flg22 treatment enhances its interaction with PARPs and PARGs and subsequently its PARylation. Consistently, the mutation of the PARylation sites in UBC13B^{4E} or treatment with PARP inhibitor 3-AB reduced its interaction with PARP2, leading to compromised PARylation of UBC13. Furthermore, we found that the overall level of K63-linked ubiquitination was induced by PAMPs and was dramatically reduced in the *parp2* and *parp1 parp2* mutants. Thus, PAMP-induced K63-linked ubiquitination is largely PARP-dependent. Therefore, we propose that, upon PAMP perception, PARP1 and PARP2 are likely activated (Feng et al., 2016) and lead to UBC13 PARylation, which in turn enhances its interaction with PARP1 and PARP2 and facilitates K63-linked ubiquitination.

In response to pathogen attack, plants produce a diverse repertoire of antimicrobial proteins to kill or limit the growth of pathogens. Secretion of PR proteins represents a major defense mechanism against pathogens, and disruption of the secretory pathway led to compromised PR protein secretion and impaired defense responses (Wang et al., 2005; Kalde et al., 2007; Wang and Dong, 2011; Pajerowska-Mukhtar et al., 2012). We have previously shown that the *parp* mutants are more susceptible to the virulent bacterial pathogen *Pst* DC3000 (Feng et al., 2015; Song et al., 2015). Here we report that the *ubc13a ubc13b* double mutant also displayed enhanced disease susceptibility to *Pst* DC3000, consistent with a previous study (Turek et al., 2018). Furthermore, the *parp2*, *parp1 parp2*, and *ubc13a ubc13b* mutants are compromised in flg22-or SA-induced resistance against *Pst* DC3000. Surprisingly, these mutants exhibited an unexpected increased accumulation of *PR1* gene transcript and protein upon induction. Even without any treatment, the expression of *PR1* gene and its product in the *ubc13a ubc13b* mutant is higher than that in WT plants. After examining the PR1 levels in the apoplastic fluid, we showed that the *parp* and *ubc13a ubc13b* mutants displayed similarly reduced secretion of PR1 protein, which likely accounts for the compromised resistance in these mutants, suggesting that PARylation and K63-linked ubiquitination cooperatively regulate plant immunity via modulation of the ERQC pathway. As an E2 ubiquitin-conjugating enzyme, UBC13A was shown to interact with several E3 ligases, including PUB20, PUB22, and PUB24, the latter two of which negatively regulate PTI, suggesting that UBC13 acts in concert with these E3s to mediate K63-linked ubiquitination and modulate immune responses (Trujillo et al., 2008; Turek et al., 2018).

Emerging evidence implies that secretion-related proteins are under PARylation and/or K63-linked ubiquitination in eukaryotes. Several PDIs, including PDIA3, PDIA5, PDIA6, P4HB, and SEC61G, were identified as PARP targets (Gagne et al., 2012; Gibson et al., 2016; Martello et al., 2016; Westcott et al., 2017). Recently, a collection of over 100 proteins involved in multiple biological processes were identified in Arabidopsis by a K63-linked ubiquitin sensor-based proteomic approach. Interestingly, about 32% of proteins under the control of K63-linked ubiquitination are related to UPR and vesicular trafficking, which are directly involved in or regulate the secretory pathway (Johnson and Vert, 2016; Romero-Barrios et al., 2020). Multiple lines of evidence indicate that the secretory pathway plays an essential role in plant immunity. A subset of NPR1-regulated proteins that are involved in translocation, folding, and maturation of secretory proteins in the ER are required for secretion of the antimicrobial PR proteins (Wang et al., 2005). Mutation in MEMB12, a Golgi-localized SNAR protein, promotes the secretion of PR1, leading to enhanced resistance to both virulent and avirulent *Pst* DC3000 (Zhang et al., 2011a). Silencing of SYP132, a plasma membrane syntaxin, inhibited the accumulation of PR1 in the extracellular space, resulting in impaired immunity (Kalde et al., 2007). As essential components of the ERQC pathway, PDI catalyzes thiol-disulfide exchanges, thus facilitating the formation, breakage, and rearrangement of disulfide bonds. PDIs have been shown to be implicated in plant immune responses. A *PDI* gene positively regulates powdery mildew resistance through interaction with an E3 ubiquitin ligase in wheat (Faheem et al., 2016). Another wheat *PDI* gene is highly induced by a hemibiotrophic fungal pathogen, and its expression is tightly

Please cite this article in press as: Yao et al., Coordinated regulation of plant immunity by poly(ADP-ribosyl)ation and K63-linked ubiquitination, Molecular Plant (2021), https://doi.org/10.1016/j.molp.2021.08.013

correlated with the levels of defense-related genes, including *PR1*, *PR2*, and *PR5* (Ray et al., 2003).

We show that Arabidopsis PDIs associate with PARP and PARG proteins and are PARylated *in vivo*. PAMP treatment promotes these interactions and PARylation of PDIs. In addition, PDIs are K63-linked ubiquitinated, and this modification is suppressed by the PARP inhibitor 3-AB. A considerable number of studies have revealed the role of PAR chains to act as scaffolds to recruit multiple proteins by noncovalent interactions and assemble signaling complexes, including the PAR-dependent recruitment of repair proteins and formation of signalosomes to facilitate repair at the sites of DNA damage (Stilmann et al., 2009; Kalisch et al., 2012; Leung, 2014; Gupte et al., 2017). It is likely that upon induction, PARP proteins recruit UBC13 and its substrates, such as PDIs, through PARylation, which facilitates K63 ubiquitination of these substrates. Importantly, we found that PDI activity is reduced in the *parp1 parp2* and *ubc13a ubc13b* mutants. Thus, we propose that PARylation and K63-linked ubiquitination of PDIs contribute to their enzymatic activities. It remains to be determined whether the other secretory pathway proteins are coregulated by PARylation and K63-linked ubiquitination. It has been reported that PDI proteins are modified by various posttranslational modifications, including S-nitrosylation, ubiquitination, and phosphorylation (Barati et al., 2006; Uehara et al., 2006; Faheem et al., 2016). Nitric oxide-mediated S-nitrosylation of a human PDI inhibits its enzymatic activity and abrogates its ability to remove the abnormal accumulation of misfolded proteins associated with neurodegenerative diseases (Uehara et al., 2006). A wheat PDI protein interacts with and is monoubiquitinated by an E3 ubiquitin ligase CMPG1, which contributes to powdery mildew resistance (Faheem et al., 2016). However, the biological significance of ubiquitination and phosphorylation and their impacts on the enzymatic activity of PDIs are not defined. Further studies are required to determine the roles of these posttranslational modifications and their interplay with PARylation and K63-linked ubiquitination.

ERQC ensures that client proteins are properly folded and delivered to sites of action through the secretory pathway (Trombetta and Parodi, 2003; Anelli and Sitia, 2008; Sun and Brodsky, 2019). Dysfunctional ERQC causes the accumulation of misfolded or unfolded proteins in the ER, which are subjected to ER-associated degradation (ERAD) (Meusser et al., 2005; Liu and Howell, 2010). A shortage of the ERQC components BIPs impairs the function of ERQC, whereas an excess of BIPs also abrogates secretion (Dorner et al., 1992). The increased expression of ERQC genes in the *parp* and *ubc13a ubc13b* mutants indicates that ERQC is defective when PARylation or K63-linked ubiquitination is compromised. The heightened accumulation of intracellular PR1 protein and the dramatically reduced level of extracellular secreted PR1 in the *parp* or *ubc13a ubc13b* mutants are likely attributed to the ER stress that has exceeded the ERQC capacity or a defective ERAD in the absence of either of the two posttranslational modifications. Alternatively, the compromised PR1 secretion may indicate that the secretory pathway is disrupted, as evidenced by the identification of SYP122 and SYP132, two components of the secretory pathway, as targets of UBC13 (Johnson and Vert, 2016; Romero-Barrios et al., 2020). Furthermore, knockdown of SYP132 resulted in a markedly reduced secretion of PR in the leaves of *N. benthamiana* plants inoculated with *P. syringae*, as in the *parp* and *ubc13a ubc13b* mutants (Kalde et al., 2007).

Based on our results, we propose that in response to PAMPs or pathogens, PARP proteins recruit UBC13 and PDIs through physical interaction and PARylation, which in turn facilitates K63-linked ubiquitination of PDIs mediated by UBC13 to activate PDIs. Subsequently, PDIs work cooperatively with other secretory proteins to fulfill their distinct functions to ensure proper protein folding and secretion into the extracellular space (Figure 7G). Taken together, our results demonstrated that UBC13 is PARylated in response to PAMP and PARylation of UBC13 promotes K63-linked ubiquitination of its substrates. Furthermore, PDIs that play a critical role in proper folding for secretion of PR proteins are coordinately regulated by PARylation and K63-linked ubiquitination. These findings bridge a critical gap between PARylation and K63-linked ubiquitination in the immune signaling pathway. Given that PARylation and ubiquitination pathways are conserved in eukaryotes and UBC13 is targeted by PARP1 in humans, similar cooperative regulatory mechanisms may also exist in other organisms and modulate diverse cellular processes other than innate immunity.

METHODS

Yeast two-hybrid screen and interaction assay

Arabidopsis PARG2 cDNA was cloned into the pGBKT7 vector and transformed into the yeast strain Y187. Yeast two-hybrid screen was performed by mating yeast strains expressing PARG2 with a pretransformed Arabidopsis cDNA library in the yeast strain AH109 as previously described (Hughes et al., 2012). The mated yeast cells were selected on SD-Leu-Trp-His-Ade plates.

To confirm interaction in yeast, bait cDNAs were cloned into the pGBKT7 vector, and prey cDNAs were cloned into the pGADT7 vector. Both prey and bait constructs were transformed into the yeast strain AH109 and plated on SD-Leu-Trp medium. Protein-protein interactions were determined by the growth of yeast on SD-Leu-Trp-His-Ade medium.

Plant materials and growth conditions

Arabidopsis plants were grown in Metro-Mix 360 soil (Sun Gro Horticulture, Agawam, MA) or were cultivated on Murashige-Skoog (MS) agar medium at 22°C under a 16-h light/8-h dark photoperiod.

The homozygous Arabidopsis T-DNA insertion lines *parp1* (GABI_380E06), *parp2* (GABI_420G03), and *parp1 parp2* have been described previously (Song et al., 2015). The T-DNA insertion lines *ubc13a-1* (WiscDsLox323H12) and *ubc13b-2* (GABI_836B11) were obtained from the Arabidopsis Biological Resource Center (ABRC). Homozygous *ubc13a ubc13b* double mutants were obtained from crosses of single mutants and were identified with allele-specific primers. The *ubc13b-1* (SALK_047381) and the *ubc13a-1 ubc13b-1* mutants have been described previously (Li and Schmidt, 2010; Turek et al., 2018; Wang et al., 2019).

Immunoblot analysis

Total proteins were prepared from Arabidopsis plants in extraction buffer (50 mM Tris-HCl, pH 7.5, 150 mM NaCl, 5 mM EDTA, 0.5% Triton X-100, 10% glycerol, and plant protease inhibitor cocktail at 1:100), separated by SDS-PAGE, transferred to nitrocellulose membranes (GE Healthcare), and probed with the K63 linkage-specific antibody (Sigma) at 1:1000, anti-pan-ADP-ribose binding reagent (anti-pan-ADPR) (MABE1016, EMD Millipore) at 1:1000, or anti-UBC13 antibody (4E11, Thermo Scientific) at 1:3000.

Please cite this article in press as: Yao et al., Coordinated regulation of plant immunity by poly(ADP-ribosyl)ation and K63-linked ubiquitination, Molecular Plant (2021), https://doi.org/10.1016/j.molp.2021.08.013

Coimmunoprecipitation assay

The cDNAs of *PARP1*, *PARP2*, *PARG1*, *PARG2*, *UBC13A*, *UBC13B*, *PDI1*, *PDI2*, *PDI3*, and *PDI4* were cloned into the Gateway destination vector pGWB405 with a C-terminal GFP tag and/or pGWB417 with a C-terminal 4×myc tag, and the resulting constructs were transformed into *Agrobacterium tumefaciens* GV3101(pMP90). Leaves of 3- to 4-week-old *N. benthamiana* plants were agroinfiltrated with Agrobacterium cultures at an OD_{600} of 0.4. For flg22 treatment, 1 μM flg22 was infiltrated into leaves 1 h prior to harvest. Samples were harvested 2 days after agroinfiltration, and total proteins were prepared in extraction buffer (50 mM Tris-HCl, pH 7.5, 150 mM NaCl, 5 mM EDTA, 0.2% Triton X-100, 10% glycerol, and plant protease inhibitor cocktail at 1:100). Immunoprecipitation was carried out with GFP-Trap magnetic beads (ChromoTek) at 4°C for 1 h with gentle rotation, followed by three washes with extraction buffer without protease inhibitors. The precipitated proteins were eluted with the SDS loading buffer, subjected to SDS-PAGE, immunoblotted with anti-myc (BioLegend) or anti-GFP (TaKaRa) antibody, and detected using SuperSignal West Dura or Femto Chemiluminescent Substrates (Thermo Scientific).

In vitro and *in vivo* PARylation assay

For *in vitro* PARylation assay, MBP-PARP1, MBP-PARP2, HIS-UBC13A, or HIS-UBC13B recombinant proteins were expressed in the *E. coli Rosetta* strain and purified with Amylose Resin High Flow (NEB) or HisPur™ Ni-NTA Superflow Agarose (Thermo Scientific) according to the manufacturer's manuals. Five hundred nanograms of MBP-PARP1 or MBP-PARP2 were incubated in 100 μL of PARylation buffer (50 mM Tris-HCl, pH 8.0, 50 mM NaCl, 10 mM $MgCl_2$) with 0.2 mM NAD^+, 1× activated DNA (Trevigen), and 1 μg of HIS-UBC13A or HIS-UBC13B at room temperature for 3 h. PARylated proteins were detected by immunoblotting using an anti-pan-ADPR reagent (MABE1016, EMD Millipore).

For *in vivo* PARylation assay of UBC13B, PDI1, and PDI3, their cDNAs were cloned into pGWB405 with a GFP tag at the C-terminus and expressed in *N. benthamiana*. Total proteins were extracted and immunoprecipitated with GFP-Trap magnetic beads, eluded with SDS loading buffer, separated on SDS-PAGE, immunoblotted with the anti-pan-ADPR reagent, and detected using SuperSignal West Dura or Femto Chemiluminescent Substrates (Thermo Scientific).

Identification of PARylation sites by mass spectrometry

To identify the PARylation sites of UBC13B, PDI1, PDI2, PDI3, and PDI4, 500 ng of MBP-PARP2 was incubated with 1 μg of HIS-UBC13B or MBP-PDI proteins in PARylation buffer (50 mM Tris-HCl, pH 8.0, 50 mM NaCl, 10 mM $MgCl_2$, and 1× activated DNA with 0.2 mM NAD^+) for 6 h at room temperature. Hydroxylamine (NH_2OH, 1 M) was then added to the reaction and incubated overnight at room temperature on a rotator to remove the poly(ADP-ribose) chain from PARylated residues. This treatment produces a hydroxamic acid derivative of a PARylated Glu or Asp residue, which has a characteristic 15.0109 Da mass signature and can be detected by mass spectrometry. Hydroxylamine-treated proteins were separated on 10% SDS-PAGE by electrophoresis. Gel slices containing unmodified and modified proteins were cut out and sent to the Proteomics Core Facility (University of Texas Southwestern Medical Center, Dallas, Texas) for mass spectrometry analysis as previously reported (Zhang et al., 2013; Feng et al., 2016). Briefly, the gel slices were digested with trypsin (Pierce) overnight, reduced by DTT, and alkylated by iodoacetamide (Sigma). Samples were cleaned up by a solid-phase extraction using an Oasis HLB plate (Waters) and subsequently injected onto an Orbitrap Elite mass spectrometer (Thermo Electron) coupled to an Ultimate 3000 nano HPLC chromatography system (Dionex). Separation of peptides was performed on a 75 μm i.d. × 50-cm EasySpray column (Thermo) at 250 nL/min by a 60-min linear gradient of 1% to 28% buffer B in buffer A. Buffer A consisted of 2% (v/v) ACN and 0.1% formic acid in water, and buffer B consisted of 80% (v/v) ACN, 10% (v/v) trifluoroethanol, and 0.1% formic acid in water. The mass spectrometer was operated in a positive ion mode with a source voltage of 2.4 kV and a capillary temperature of 275°C. MS scans were performed at a resolution of 240,000 in the Orbitrap, and up to 14 MS/MS spectra were acquired using collisionally induced dissociation (CID) for ions with charges two or higher. The charge exclusion was set to exclude the unassigned and charge one species with a dynamic exclusion of 15 s.

Raw MS data were analyzed using Proteome Discoverer v2.2 (Thermo). Fragment and precursor tolerances were set to 0.6 Da and 10 ppm, respectively, with three missed cleavages allowed. Carbamidomethylation of Cys was set as a fixed modification, whereas oxidation of Met and hydroxamic acid modification (+15.0109 Da) of Asp and Glu were set as variable modifications. The peptide false-discovery rate was set to 1%. The raw mass spectrometry proteomics data have been deposited to MassIVE (https://massive.ucsd.edu) with the dataset identifier MSV000087876.

RNA isolation and qRT-PCR

For RNA isolation, 10-day-old seedlings grown on 1/2 MS plates were transferred to 2 mL H_2O in a six-well plate to recover for 1 day, and then treated with 1 μM flg22 for indicated times. RNA was extracted using the Plant RNeasy Kit with DNase I treatment (Qiagen), and first strand cDNAs were synthesized using Superscript II reverse transcriptase (Invitrogen). qRT-PCR was performed using SYBR Green PCR Master Mix on the QuantStudio six Flex real-time PCR system (Applied Biosystems). *UBQ5* was used as an internal control. Error bars represent SD from three biological replicates. Primers used in this study are listed in Supplemental Table 2.

ROS assay

Leaf discs were collected from 3-week-old plants, and each disc was placed in a well with 50 μL of 1% DMSO solution in a 96-well plate. After overnight incubation, DMSO was then replaced by 50 μL of elicitation solution containing 1 μM flg22, 0.1 mg/mL luminol (Sigma), and 0.1 mg/mL horseradish peroxidase (Sigma). Luminescence was measured immediately with a 2-min interval over a 35-min period using the Fluoroskan FL Microplate Fluorometer and Luminometer (Thermo Fisher).

Callose deposition assay

Seven-day-old seedlings grown on 1/2 MS plates were treated with 1 μM flg22 for 24 h. After fixing overnight in an FAA solution (10% formaldehyde, 5% acetic acid, and 50% ethanol), seedlings were cleared in 95% ethanol and stained with 0.01% aniline blue in 67 mM K_2HPO_4 (pH 12). The callose deposits on entire cotyledons were visualized with the Nikon Eclipse 90i Fluorescence Microscope and quantified using ImageJ software.

MAPK assay

Ten-day-old seedlings grown on 1/2 MS plates were transferred into a six-well tissue culture plate containing 2 mL H_2O per well. After 24-h incubation, seedlings were treated with 1 μM flg22 for 5, 15, and 45 min. Total proteins were extracted and separated on 12% SDS-PAGE. The phosphorylated MAPKs were detected with anti-pERK antibody (Cell Signaling).

Bacterial growth assay

Three-week-old Arabidopsis plants were inoculated with *Pst* DC3000 at an OD_{600} of 0.0005. Three days postinoculation, leaf discs were sampled from inoculated plants and homogenized by mechanical disruption in 10 mM $MgCl_2$. Samples were diluted serially and plated on NYGA plates with appropriate antibiotics. The colony-forming units were counted 2 days after incubation at 28°C. For flg22-induced resistance assay, 3-week-old plants were infiltrated with 1 μM flg22. Four hours after treatment, inoculated leaves were challenged with *Pst* DC3000 at an OD_{600} of 0.001. Three days postinoculation, bacterial numbers were determined as described above. For SA-induced resistance assay, 3-week-old Arabidopsis plants were pretreated with 1 mM SA for 24 h and subsequently inoculated with *Pst* DC3000 at an OD_{600} of 0.001. Three days postinoculation, bacterial numbers were determined as described above.

Please cite this article in press as: Yao et al., Coordinated regulation of plant immunity by poly(ADP-ribosyl)ation and K63-linked ubiquitination, Molecular Plant (2021), https://doi.org/10.1016/j.molp.2021.08.013

Secreted PR1 protein assay

Three-week-old Arabidopsis plants were infiltrated with *Pst* DC3000 at an OD_{600} of 0.02. Three days postinoculation, inoculated leaves were collected and vacuumed in a solution containing 100 mM Tris-HCl, pH 7.8, 500 mM sucrose, 10 mM $MgCl_2$, 10 mM $CaCl_2$, 1 mM phenylmethylsulfonyl fluoride, and 1 mM β-mercaptoethanol. Secreted proteins were collected by centrifuging the infiltrated leaf tissues that were placed in a syringe for 5 min at 1500 × *g*. Total protein was extracted as described above. Total and secreted proteins were separated on SDS-PAGE and immunoblotted with anti-PR1 antibody.

PDI activity assay

One gram of 10-day-old Arabidopsis seedlings was ground in liquid nitrogen and suspended in 1 mL of suspension buffer (25 mM Tris-HCl, pH 7.5, 0.25 M sucrose, 2 mM EDTA, 2 mM DTT, 15 mM β-mercaptoethanol, 10% glycerol, and proteinase inhibitor cocktail). After removing cell debris by centrifuging at 10,000 × *g* for 20 min at 4°C, Triton X-100 was added to a final concentration of 1% (v/v) to release proteins from membrane fractions. Total proteins were collected and quantified by the Bradford assay (Bio-Rad). An equal amount of proteins from different samples was used to determine PDI activity using the PDI Activity Assay Kit (Biovision) according to the manufacturer's instructions.

SUPPLEMENTAL INFORMATION

Supplemental information is available at *Molecular Plant Online*.

FUNDING

This work was supported by a start-up fund from Texas A&M AgriLife Research to J.S. and a grant from the National Science Foundation (IOS-1951094) to P.H. and J.S.

AUTHOR CONTRIBUTIONS

J.S. and D.Y. conceived and designed the experiments. D.Y. and M.A. performed the experiments and acquired the data. D.Y., J.S., P.H., and A.B. analyzed the data. D.Y. and J.S. wrote the paper with input from all authors.

ACKNOWLEDGMENTS

We thank Dr. Wei Xiao for providing the *ubc13a-1 ubc13b-1* double mutant. No conflict of interest declared.

Received: January 6, 2021
Revised: May 24, 2021
Accepted: August 15, 2021
Published: August 17, 2021

REFERENCES

Adams-Phillips, L., Briggs, A.G., and Bent, A.F. (2010). Disruption of poly(ADP-ribosyl)ation mechanisms alters responses of Arabidopsis to biotic stress. Plant Physiol. **152**:267–280.

Andersen, P.L., Xu, F., and Xiao, W. (2008). Eukaryotic DNA damage tolerance and translesion synthesis through covalent modifications of PCNA. Cell Res. **18**:162–173.

Andersen, P.L., Zhou, H., Pastushok, L., Moraes, T., McKenna, S., Ziola, B., Ellison, M.J., Dixit, V.M., and Xiao, W. (2005). Distinct regulation of Ubc13 functions by the two ubiquitin-conjugating enzyme variants Mms2 and Uev1A. J. Cell Biol. **170**:745–755.

Anelli, T., and Sitia, R. (2008). Protein quality control in the early secretory pathway. EMBO J. **27**:315–327.

Arrano-Salinas, P., Dominguez-Figueroa, J., Herrera-Vasquez, A., Zavala, D., Medina, J., Vicente-Carbajosa, J., Meneses, C., Canessa, P., Moreno, A.A., and Blanco-Herrera, F. (2018). WRKY7, -11 and -17 transcription factors are modulators of the bZIP28 branch of the unfolded protein response during PAMP-triggered immunity in Arabidopsis thaliana. Plant Sci. **277**:242–250.

Bai, P. (2015). Biology of poly(ADP-ribose) polymerases: the factotums of cell maintenance. Mol. Cell **58**:947–958.

Balmant, K.M. (2016). Redox Proteomics of Plant Innate Immunity in Stomatal Guard Cells (University of Florida).

Barati, M.T., Rane, M.J., Klein, J.B., and McLeish, K.R. (2006). A proteomic screen identified stress-induced chaperone proteins as targets of Akt phosphorylation in mesangial cells. J. Proteome Res. **5**:1636–1646.

Bock, F.J., Todorova, T.T., and Chang, P. (2015). RNA regulation by poly(ADP-ribose) polymerases. Mol. Cell **58**:959–969.

Boller, T., and Felix, G. (2009). A renaissance of elicitors: perception of microbe-associated molecular patterns and danger signals by pattern-recognition receptors. Annu. Rev. Plant Biol. **60**:379–406.

Briggs, A.G., and Bent, A.F. (2011). Poly(ADP-ribosyl)ation in plants. Trends Plant Sci. **16**:372–380.

Chen, Z.J. (2012). Ubiquitination in signaling to and activation of IKK. Immunol. Rev. **246**:95–106.

Cho, E.J., Yuen, C.Y., Kang, B.H., Ondzighi, C.A., Staehelin, L.A., and Christopher, D.A. (2011). Protein disulfide isomerase-2 of Arabidopsis mediates protein folding and localizes to both the secretory pathway and nucleus, where it interacts with maternal effect embryo arrest factor. Mol. Cells **32**:459–475.

D'Amours, D., Desnoyers, S., D'Silva, I., and Poirier, G.G. (1999). Poly(ADP-ribosyl)ation reactions in the regulation of nuclear functions. Biochem. J. **342**:249–268.

Date, H., Igarashi, S., Sano, Y., Takahashi, T., Takahashi, T., Takano, H., Tsuji, S., Nishizawa, M., and Onodera, O. (2004). The FHA domain of aprataxin interacts with the C-terminal region of XRCC1. Biochem. Biophys. Res. Commun. **325**:1279–1285.

De Vos, M., El Ramy, R., Quenet, D., Wolf, P., Spada, F., Magroun, N., Babbio, F., Schreiber, V., Leonhardt, H., Bonapace, I.M., et al. (2014). Poly(ADP-ribose) polymerase 1 (PARP1) associates with E3 ubiquitin-protein ligase UHRF1 and modulates UHRF1 biological functions. J. Biol. Chem. **289**:16223–16238.

Denoux, C., Galletti, R., Mammarella, N., Gopalan, S., Werck, D., De Lorenzo, G., Ferrari, S., Ausubel, F.M., and Dewdney, J. (2008). Activation of defense response pathways by OGs and Flg22 elicitors in Arabidopsis seedlings. Mol. Plant **1**:423–445.

Deruyffelaere, C., Bouchez, I., Morin, H., Guillot, A., Miquel, M., Froissard, M., Chardot, T., and D'Andrea, S. (2015). Ubiquitin-mediated proteasomal degradation of oleosins is involved in oil body mobilization during post-germinative seedling growth in arabidopsis. Plant Cell Physiol. **56**:1374–1387.

Dodds, P.N., and Rathjen, J.P. (2010). Plant immunity: towards an integrated view of plant-pathogen interactions. Nat. Rev. Genet. **11**:539–548.

Dorner, A.J., Wasley, L.C., and Kaufman, R. (1992). Overexpression of GRP78 mitigates stress induction of glucose regulated proteins and blocks secretion of selective proteins in Chinese hamster ovary cells. EMBO J. **11**:1563–1571.

Faheem, M., Li, Y., Arshad, M., Jiangyue, C., Jia, Z., Wang, Z., Xiao, J., Wang, H., Cao, A., Xing, L., et al. (2016). A disulphide isomerase gene (PDI-V) from Haynaldia villosa contributes to powdery mildew resistance in common wheat. Sci. Rep. **6**:24227.

Feige, M.J., and Hendershot, L.M. (2011). Disulfide bonds in ER protein folding and homeostasis. Curr. Opin. Cell Biol. **23**:167–175.

Feng, B., Liu, C., de Oliveira, M.V., Intorne, A.C., Li, B., Babilonia, K., de Souza Filho, G.A., Shan, L., and He, P. (2015). Protein poly(ADP-ribosyl)ation regulates arabidopsis immune gene expression and defense responses. PLoS Genet. **11**:e1004936.

Feng, B., Ma, S., Chen, S., Zhu, N., Zhang, S., Yu, B., Yu, Y., Le, B., Chen, X., Dinesh-Kumar, S.P., et al. (2016). PARylation of the

Please cite this article in press as: Yao et al., Coordinated regulation of plant immunity by poly(ADP-ribosyl)ation and K63-linked ubiquitination, Molecular Plant (2021), https://doi.org/10.1016/j.molp.2021.08.013

forkhead-associated domain protein DAWDLE regulates plant immunity. EMBO Rep. **17**:1799–1813.

Gagne, J.P., Pic, E., Isabelle, M., Krietsch, J., Ethier, C., Paquet, E., Kelly, I., Boutin, M., Moon, K.M., Foster, L.J., et al. (2012). Quantitative proteomics profiling of the poly(ADP-ribose)-related response to genotoxic stress. Nucleic Acids Res. **40**:7788–7805.

Gibson, B.A., and Kraus, W.L. (2012). New insights into the molecular and cellular functions of poly(ADP-ribose) and PARPs. Nat. Rev. Mol. Cell Biol. **13**:411–424.

Gibson, B.A., Zhang, Y., Jiang, H., Hussey, K.M., Shrimp, J.H., Lin, H., Schwede, F., Yu, Y., and Kraus, W.L. (2016). Chemical genetic discovery of PARP targets reveals a role for PARP-1 in transcription elongation. Science **353**:45–50.

Gomez-Gomez, L., and Boller, T. (2000). FLS2: an LRR receptor-like kinase involved in the perception of the bacterial elicitor flagellin in Arabidopsis. Mol. Cell **5**:1003–1011.

Gruber, C.W., Cemazar, M., Heras, B., Martin, J.L., and Craik, D.J. (2006). Protein disulfide isomerase: the structure of oxidative folding. Trends Biochem. Sci. **31**:455–464.

Gupte, R., Liu, Z., and Kraus, W.L. (2017). PARPs and ADP-ribosylation: recent advances linking molecular functions to biological outcomes. Genes Dev. **31**:101–126.

Hassa, P.O., Haenni, S.S., Elser, M., and Hottiger, M.O. (2006). Nuclear ADP-ribosylation reactions in mammalian cells: where are we today and where are we going? Microbiol. Mol. Biol. Rev. **70**:789–829.

Hinz, M., Stilmann, M., Arslan, S.C., Khanna, K.K., Dittmar, G., and Scheidereit, C. (2010). A cytoplasmic ATM-TRAF6-cIAP1 module links nuclear DNA damage signaling to ubiquitin-mediated NF-kappaB activation. Mol. Cell **40**:63–74.

Hochstrasser, M. (1996). Ubiquitin-dependent protein degradation. Annu. Rev. Genet. **30**:405–439.

Hofmann, R.M., and Pickart, C.M. (1999). Noncanonical MMS2-encoded ubiquitin-conjugating enzyme functions in assembly of novel polyubiquitin chains for DNA repair. Cell **96**:645–653.

Hughes, R.M., Vrana, J.D., Song, J., and Tucker, C.L. (2012). Light-dependent, dark-promoted interaction between Arabidopsis cryptochrome 1 and phytochrome B proteins. J. Biol. Chem. **287**:22165–22172.

Iwai, K. (2012). Diverse ubiquitin signaling in NF-kappaB activation. Trends Cell Biol. **22**:355–364.

Johnson, A., and Vert, G. (2016). Unraveling K63 polyubiquitination networks by sensor-based proteomics. Plant Physiol. **171**:1808–1820.

Jones, J.D., and Dangl, J.L. (2006). The plant immune system. Nature **444**:323–329.

Kalde, M., Nuhse, T.S., Findlay, K., and Peck, S.C. (2007). The syntaxin SYP132 contributes to plant resistance against bacteria and secretion of pathogenesis-related protein 1. Proc. Natl. Acad. Sci. U S A **104**:11850–11855.

Kalisch, T., Ame, J.C., Dantzer, F., and Schreiber, V. (2012). New readers and interpretations of poly(ADP-ribosyl)ation. Trends Biochem. Sci. **37**:381–390.

Kang, H.C., Lee, Y.I., Shin, J.H., Andrabi, S.A., Chi, Z., Gagne, J.P., Lee, Y., Ko, H.S., Lee, B.D., Poirier, G.G., et al. (2011). Iduna is a poly(ADP-ribose) (PAR)-dependent E3 ubiquitin ligase that regulates DNA damage. Proc. Natl. Acad. Sci. U S A **108**:14103–14108.

Kasai, K., Takano, J., Miwa, K., Toyoda, A., and Fujiwara, T. (2011). High boron-induced ubiquitination regulates vacuolar sorting of the BOR1 borate transporter in Arabidopsis thaliana. J. Biol. Chem. **286**:6175–6183.

Kleffmann, T., Russenberger, D., von Zychlinski, A., Christopher, W., Sjolander, K., Gruissem, W., and Baginsky, S. (2004). The Arabidopsis thaliana chloroplast proteome reveals pathway abundance and novel protein functions. Curr. Biol. **14**:354–362.

Koivunen, P., Pirneskoski, A., Karvonen, P., Ljung, J., Helaakoski, T., Notbohm, H., and Kivirikko, K.I. (1999). The acidic C-terminal domain of protein disulfide isomerase is not critical for the enzyme subunit function or for the chaperone or disulfide isomerase activities of the polypeptide. EMBO J. **18**:65–74.

Lamb, R.S., Citarelli, M., and Teotia, S. (2012). Functions of the poly(ADP-ribose) polymerase superfamily in plants. Cell. Mol. Life Sci **69**:175–189.

Le May, N., Iltis, I., Ame, J.C., Zhovmer, A., Biard, D., Egly, J.M., Schreiber, V., and Coin, F. (2012). Poly (ADP-ribose) glycohydrolase regulates retinoic acid receptor-mediated gene expression. Mol. Cell **48**:785–798.

Leitner, J., Petrasek, J., Tomanov, K., Retzer, K., Parezova, M., Korbei, B., Bachmair, A., Zazimalova, E., and Luschnig, C. (2012). Lysine63-linked ubiquitylation of PIN2 auxin carrier protein governs hormonally controlled adaptation of Arabidopsis root growth. Proc. Natl. Acad. Sci. U S A **109**:8322–8327.

Leung, A.K. (2014). Poly(ADP-ribose): an organizer of cellular architecture. J. Cell Biol. **205**:613–619.

Li, P., Huang, P., Li, X., Yin, D., Ma, Z., Wang, H., and Song, H. (2018). Tankyrase mediates K63-linked ubiquitination of JNK to confer stress tolerance and influence lifespan in Drosophila. Cell Rep. **25**:437–448.

Li, W., and Schmidt, W. (2010). A lysine-63-linked ubiquitin chain-forming conjugase, UBC13, promotes the developmental responses to iron deficiency in Arabidopsis roots. Plant J. **62**:330–343.

Liu, J.-X., and Howell, S.H. (2010). Endoplasmic reticulum protein quality control and its relationship to environmental stress responses in plants. Plant Cell **22**:2930–2942.

Lu, D.P., and Christopher, D.A. (2008). Endoplasmic reticulum stress activates the expression of a sub-group of protein disulfide isomerase genes and AtbZIP60 modulates the response in Arabidopsis thaliana. Mol. Genet. Genomics **280**:199–210.

Lucero, H.A., and Kaminer, B. (1999). The role of calcium on the activity of ERcalcistorin/protein-disulfide isomerase and the significance of the C-terminal and its calcium binding. A comparison with mammalian protein-disulfide isomerase. J. Biol. Chem. **274**:3243–3251.

Luo, X., and Kraus, W.L. (2012). On PAR with PARP: cellular stress signaling through poly(ADP-ribose) and PARP-1. Genes Dev. **26**:417–432.

Macho, A.P., and Zipfel, C. (2014). Plant PRRs and the activation of innate immune signaling. Mol. Cell **54**:263–272.

Martello, R., Leutert, M., Jungmichel, S., Bilan, V., Larsen, S.C., Young, C., Hottiger, M.O., and Nielsen, M.L. (2016). Proteome-wide identification of the endogenous ADP-ribosylome of mammalian cells and tissue. Nat. Commun. **7**:12917.

Martins, S., Dohmann, E.M., Cayrel, A., Johnson, A., Fischer, W., Pojer, F., Satiat-Jeunemaitre, B., Jaillais, Y., Chory, J., Geldner, N., et al. (2015). Internalization and vacuolar targeting of the brassinosteroid hormone receptor BRI1 are regulated by ubiquitination. Nat. Commun. **6**:6151.

Meusser, B., Hirsch, C., Jarosch, E., and Sommer, T. (2005). ERAD: the long road to destruction. Nat. Cell Biol. **7**:766–772.

Mishina, T.E., and Zeier, J. (2007). Pathogen-associated molecular pattern recognition rather than development of tissue necrosis contributes to bacterial induction of systemic acquired resistance in Arabidopsis. Plant J. **50**:500–513.

Mural, R.V., Liu, Y., Rosebrock, T.R., Brady, J.J., Hamera, S., Connor, R.A., Martin, G.B., and Zeng, L. (2013). The tomato Fni3 lysine-63-

specific ubiquitin-conjugating enzyme and suv ubiquitin E2 variant positively regulate plant immunity. Plant Cell **25**:3615–3631.

Nathan, J.A., and Lehner, P.J. (2009). The trafficking and regulation of membrane receptors by the RING-CH ubiquitin E3 ligases. Exp. Cell Res. **315**:1593–1600.

Pajerowska-Mukhtar, K.M., Wang, W., Tada, Y., Oka, N., Tucker, C.L., Fonseca, J.P., and Dong, X. (2012). The HSF-like transcription factor TBF1 is a major molecular switch for plant growth-to-defense transition. Curr. Biol. **22**:103–112.

Pastushok, L., Moraes, T.F., Ellison, M.J., and Xiao, W. (2005). A single Mms2 "key" residue insertion into a Ubc13 pocket determines the interface specificity of a human Lys63 ubiquitin conjugation complex. J. Biol. Chem. **280**:17891–17900.

Pellegrino, S., and Altmeyer, M. (2016). Interplay between ubiquitin, SUMO, and poly(ADP-ribose) in the cellular response to genotoxic stress. Front. Genet. **7**:63.

Peralta-Leal, A., Rodriguez-Vargas, J.M., Aguilar-Quesada, R., Rodriguez, M.I., Linares, J.L., de Almodovar, M.R., and Oliver, F.J. (2009). PARP inhibitors: new partners in the therapy of cancer and inflammatory diseases. Free Radic. Biol. Med. **47**:13–26.

Pickart, C.M. (2001). Mechanisms underlying ubiquitination. Annu. Rev. Biochem. **70**:503–533.

Ray, S., Anderson, J.M., Urmeev, F.I., and Goodwin, S.B. (2003). Rapid induction of a protein disulfide isomerase and defense-related genes in wheat in response to the hemibiotrophic fungal pathogen Mycosphaerella graminicola. Plant Mol Biol **53**:701–714. https://doi.org/10.1023/B:PLAN.0000019120.74610.52.

Rissel, D., Losch, J., and Peiter, E. (2014). The nuclear protein Poly(ADP-ribose) polymerase 3 (AtPARP3) is required for seed storability in Arabidopsis thaliana. Plant Biol. (Stuttg) **16**:1058–1064.

Romero-Barrios, N., Monachello, D., Dolde, U., Wong, A., San Clemente, H., Cayrel, A., Johnson, A., Lurin, C., and Vert, G. (2020). Advanced cataloging of lysine-63 polyubiquitin networks by genomic, interactome, and sensor-based proteomic analyses. Plant Cell **32**:123–138.

Romero-Barrios, N., and Vert, G. (2018). Proteasome-independent functions of lysine-63 polyubiquitination in plants. New Phytol. **217**:995–1011.

Saijo, Y. (2010). ER quality control of immune receptors and regulators in plants. Cell Microbiol. **12**:716–724.

Song, J., Keppler, B.D., Wise, R.R., and Bent, A.F. (2015). PARP2 is the predominant poly(ADP-ribose) polymerase in arabidopsis DNA damage and immune responses. PLoS Genet. **11**:e1005200.

Spoel, S.H., and Dong, X. (2012). How do plants achieve immunity? Defence without specialized immune cells. Nat. Rev. Immunol. **12**:89–100.

Stilmann, M., Hinz, M., Arslan, S.C., Zimmer, A., Schreiber, V., and Scheidereit, C. (2009). A nuclear poly(ADP-ribose)-dependent signalosome confers DNA damage-induced IkappaB kinase activation. Mol. Cell **36**:365–378.

Strasser, R. (2018). Protein quality control in the endoplasmic reticulum of plants. Annu. Rev. Plant Biol. **69**:147–172.

Sun, Z., and Brodsky, J.L. (2019). Protein quality control in the secretory pathway. J. Cell Biol. **218**:3171–3187.

Swatek, K.N., and Komander, D. (2016). Ubiquitin modifications. Cell Res. **26**:399–422.

Trombetta, E.S., and Parodi, A.J. (2003). Quality control and protein folding in the secretory pathway. Annu. Rev. Cell Dev. Biol. **19**:649–676.

Trujillo, M., Ichimura, K., Casais, C., and Shirasu, K. (2008). Negative regulation of PAMP-triggered immunity by an E3 ubiquitin ligase triplet in Arabidopsis. Curr. Biol. **18**:1396–1401.

Tsuda, K., Sato, M., Glazebrook, J., Cohen, J.D., and Katagiri, F. (2008). Interplay between MAMP-triggered and SA-mediated defense responses. Plant J. **53**:763–775.

Turek, I., Tischer, N., Lassig, R., and Trujillo, M. (2018). Multi-tiered pairing selectivity between E2 ubiquitin–conjugating enzymes and E3 ligases. J. Biol. Chem. **293**:16324–16336.

Uehara, T., Nakamura, T., Yao, D., Shi, Z.Q., Gu, Z., Ma, Y., Masliah, E., Nomura, Y., and Lipton, S.A. (2006). S-nitrosylated protein-disulphide isomerase links protein misfolding to neurodegeneration. Nature **441**:513–517.

Van Loon, L., and Van Strien, E. (1999). The families of pathogenesis-related proteins, their activities, and comparative analysis of PR-1 type proteins. Physiol. Mol. Plant Path. **55**:85–97.

Wang, D., and Dong, X. (2011). A highway for war and peace: the secretory pathway in plant-microbe interactions. Mol. Plant **4**:581–587.

Wang, D., Weaver, N.D., Kesarwani, M., and Dong, X. (2005). Induction of protein secretory pathway is required for systemic acquired resistance. Science **308**:1036–1040.

Wang, H., Wang, S., Lu, Y., Alvarez, S., Hicks, L.M., Ge, X., and Xia, Y. (2012). Proteomic analysis of early-responsive redox-sensitive proteins in Arabidopsis. J. Proteome Res. **11**:412–424.

Wang, L., Wen, R., Wang, J., Xiang, D., Wang, Q., Zang, Y., Wang, Z., Huang, S., Li, X., Datla, R., et al. (2019). Arabidopsis UBC13 differentially regulates two programmed cell death pathways in responses to pathogen and low-temperature stress. New Phytol. **221**:919–934.

Wen, R., Newton, L., Li, G., Wang, H., and Xiao, W. (2006). Arabidopsis thaliana UBC13: implication of error-free DNA damage tolerance and Lys63-linked polyubiquitylation in plants. Plant Mol. Biol. **61**:241–253.

Wen, R., Wang, S., Xiang, D., Venglat, P., Shi, X., Zang, Y., Datla, R., Xiao, W., and Wang, H. (2014). UBC13, an E2 enzyme for Lys63-linked ubiquitination, functions in root development by affecting auxin signaling and Aux/IAA protein stability. Plant J. **80**:424–436.

Westcott, N.P., Fernandez, J.P., Molina, H., and Hang, H.C. (2017). Chemical proteomics reveals ADP-ribosylation of small GTPases during oxidative stress. Nat. Chem. Biol. **13**:302–308.

Wittenberg, G., Levitan, A., Klein, T., Dangoor, I., Keren, N., and Danon, A. (2014). Knockdown of the Arabidopsis thaliana chloroplast protein disulfide isomerase 6 results in reduced levels of photoinhibition and increased D1 synthesis in high light. Plant J. **78**:1003–1013.

Wu, X., and Karin, M. (2015). Emerging roles of Lys63-linked polyubiquitylation in immune responses. Immunol. Rev. **266**:161–174.

Yau, R., and Rape, M. (2016). The increasing complexity of the ubiquitin code. Nat. Cell Biol. **18**:579–586.

Yuen, C.Y., Matsumoto, K.O., and Christopher, D.A. (2013). Variation in the subcellular localization and protein folding activity among Arabidopsis thaliana homologs of protein disulfide isomerase. Biomolecules **3**:848–869.

Zhang, X., Zhao, H., Gao, S., Wang, W.C., Katiyar-Agarwal, S., Huang, H.D., Raikhel, N., and Jin, H. (2011a). Arabidopsis Argonaute 2 regulates innate immunity via miRNA393(*)-mediated silencing of a Golgi-localized SNARE gene, MEMB12. Mol. Cell **42**:356–366.

Zhang, Y., Liu, S., Mickanin, C., Feng, Y., Charlat, O., Michaud, G.A., Schirle, M., Shi, X., Hild, M., Bauer, A., et al. (2011b). RNF146 is a poly(ADP-ribose)-directed E3 ligase that regulates axin degradation and Wnt signalling. Nat. Cell Biol. **13**:623–629.

Zhang, Y., Wang, J., Ding, M., and Yu, Y. (2013). Site-specific characterization of the Asp- and glu-ADP-ribosylated proteome. Nat. Methods **10**:981–984.

Zhou, B., and Zeng, L. (2017). Conventional and unconventional ubiquitination in plant immunity. Mol. Plant Pathol. **18**:1313–1330.

Molecular Plant, Volume *14*

Supplemental information

Coordinated regulation of plant immunity by poly(ADP-ribosyl)ation and K63-linked ubiquitination

Dongsheng Yao, Marcus A. Arguez, Ping He, Andrew F. Bent, and Junqi Song

Supplemental information

Coordinated Regulation of Plant Immunity by Poly(ADP-ribosyl)ation and K63-Linked Ubiquitination

Dongsheng Yao[1], Marcus A. Arguez[1], Ping He[2], Andrew F. Bent[3], and Junqi Song[1,4*]

[1]Texas A&M AgriLife Research Center at Dallas, Texas A&M University System, Dallas, TX 75252, USA

[2]Department of Biochemistry and Biophysics, Texas A&M University, College Station, TX 77843, USA

[3]Department of Plant Pathology, University of Wisconsin-Madison, Madison, WI 53706, USA

[4]Department of Plant Pathology and Microbiology, Texas A&M University, College Station, TX 77843, USA

*Correspondence: junqi.song@ag.tamu.edu

Supplemental Figures: Figure S1-S9

Supplemental Tables: Table S1-S3

Supplemental Information

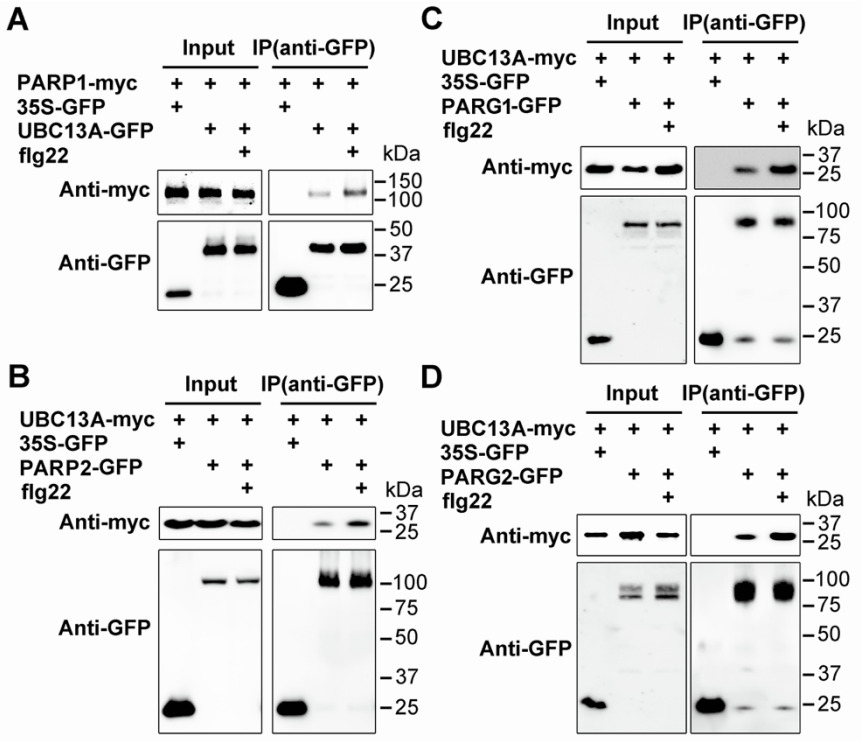

Supplemental Figure 1. UBC13A Interacts with PARP1, PARP2, PARG1, and PARG2 *In Vivo*. UBC13A-GFP was coexpressed with myc-tagged PARP1 in *N. benthamiana*. UBC13A-myc was coexpressed with GFP-tagged PARP2, PARG1, or PARG2 in *N. benthamiana*. All constructs were driven by the 35S promoter. Total proteins were extracted, immunoprecipitated GFP-Trap magnetic beads, and immunoblotted with anti-myc or anti-GFP antibody. Plants were treated without or with 1 μM flg22 for 1 h.

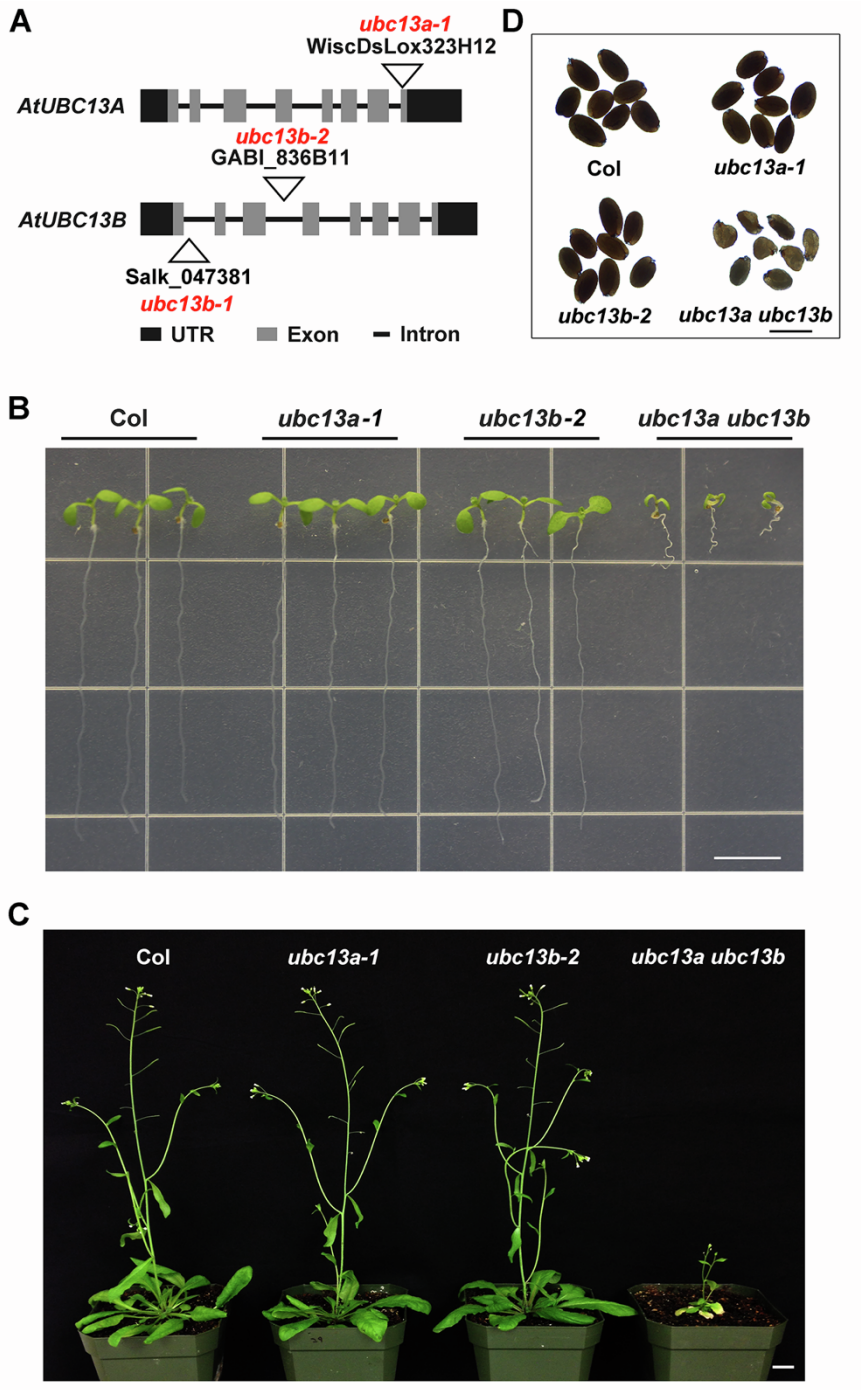

Supplemental Figure 2. Phenotypes of the *ubc13* Mutants.

(A) T-DNA insertion sites in *UBC13A* and *UBC13B*. Black boxes represent untranslated regions (UTR). Grey lines and boxes represent introns and exons, respectively.

(B) Morphology of 10-day-old WT Col and *ubc13* mutant plants. Bar = 1 cm.

(**C**)The growth phenotype of 5-week-old *ubc13a-1*, *ubc13b-2*, and *ubc13a ubc13b* mutants. Bar = 1 cm.

(D) Phenotypes of the seeds of WT Col and *ubc13* mutants. Bar = 0.02 cm.

A

#1	b⁺	b²⁺	b³⁺	Seq.	y⁺	y²⁺	y³⁺	#2
1	114.09134	57.54931	38.70196	L				19
2	227.17540	114.09134	76.39665	L	1916.91306	958.96017	639.64254	18
3	314.20743	157.60735	105.40733	S	1803.82900	902.41814	601.94785	17
4	458.26092	229.63410	153.42516	E-Hydroxamic_acid	1716.79697	858.90212	572.93718	16
5	555.31369	278.16048	185.77608	P	1572.74348	786.87538	524.91934	15
6	626.35080	313.67904	209.45512	A	1475.69072	738.34900	492.56842	14
7	723.40357	362.20542	241.80604	P	1404.65360	702.83044	468.88939	13
8	780.42503	390.71615	260.81319	G	1307.60084	654.30406	436.53846	12
9	893.50909	447.25819	298.50788	I	1250.57937	625.79333	417.53131	11
10	980.54112	490.77420	327.51856	S	1137.49531	569.25129	379.83662	10
11	1051.57824	526.29276	351.19760	A	1050.46328	525.73528	350.82595	9
12	1138.61026	569.80877	380.20827	S	979.42617	490.21672	327.14691	8
13	1235.66303	618.33515	412.55919	P	892.39414	446.70071	298.13623	7
14	1322.69506	661.85117	441.56987	S	795.34138	398.17433	265.78531	6
15	1466.74855	733.87791	489.58770	E-Hydroxamic_acid	708.30935	354.65831	236.77463	5
16	1610.80204	805.90466	537.60553	E-Hydroxamic_acid	564.25586	282.63157	188.75680	4
17	1724.84497	862.92612	575.61984	N	420.20236	210.60482	140.73897	3
18	1855.88545	928.44636	619.30000	M	306.15944	153.58336	102.72466	2
19				R	175.11895	88.06311	59.04450	1

B

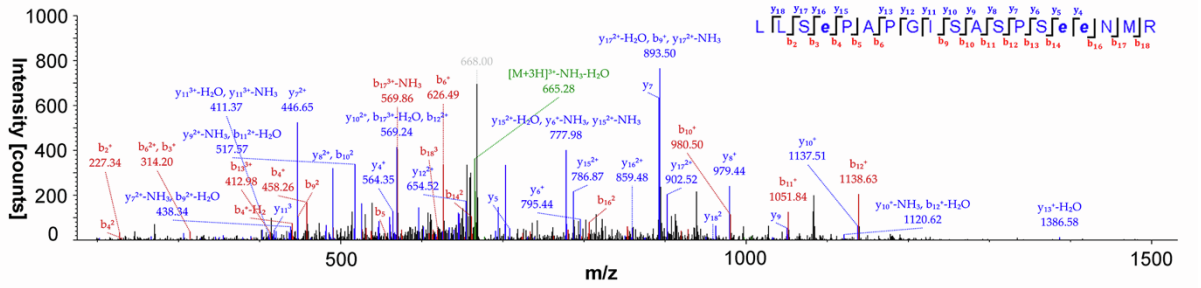

Supplemental Figure 3. Identification of PARylation Sites in UBC13A.

(A) List of the mass/charge values of b^+ ions and y^+ ions of the peptide (LELFLPEEYPMAAPK), PARylated Glu (E) sites are indicated by E-Hydroxamic_acid. The mass values in red and blue correspond to the identified b^+ ions and y^+ ions peaks in the spectrum.

(B) MS/MS spectrum of a triple charged peptide with PARylation Glu sites. The "e" in bold and lowercase indicates a modified Glu residue.

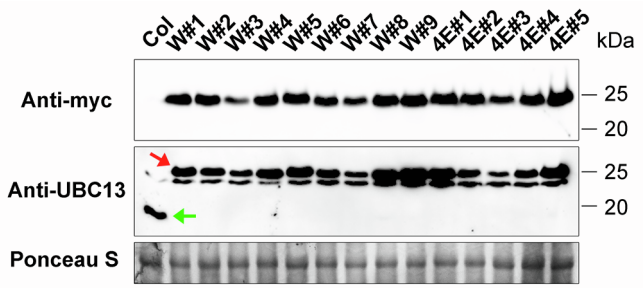

Supplemental Figure 4. Immunoblot Analysis of Transgenic Lines Expressing *UBC13B-myc* or *UBC13B^{4E}-myc* in the Homozygous *ubc13a ubc13b* Mutant Background. Total proteins were extracted from 10-day-old seedlings, separated on SDS-PAGE, immunoblotted with anti-myc or anti-UBC13 antibody. Red arrow indicates the band of UBC13B-myc or UBC13B^{4E}-myc, Green arrow indicates the band of endogenous UBC13 protein. Equal loading was confirmed by Ponceau S staining.

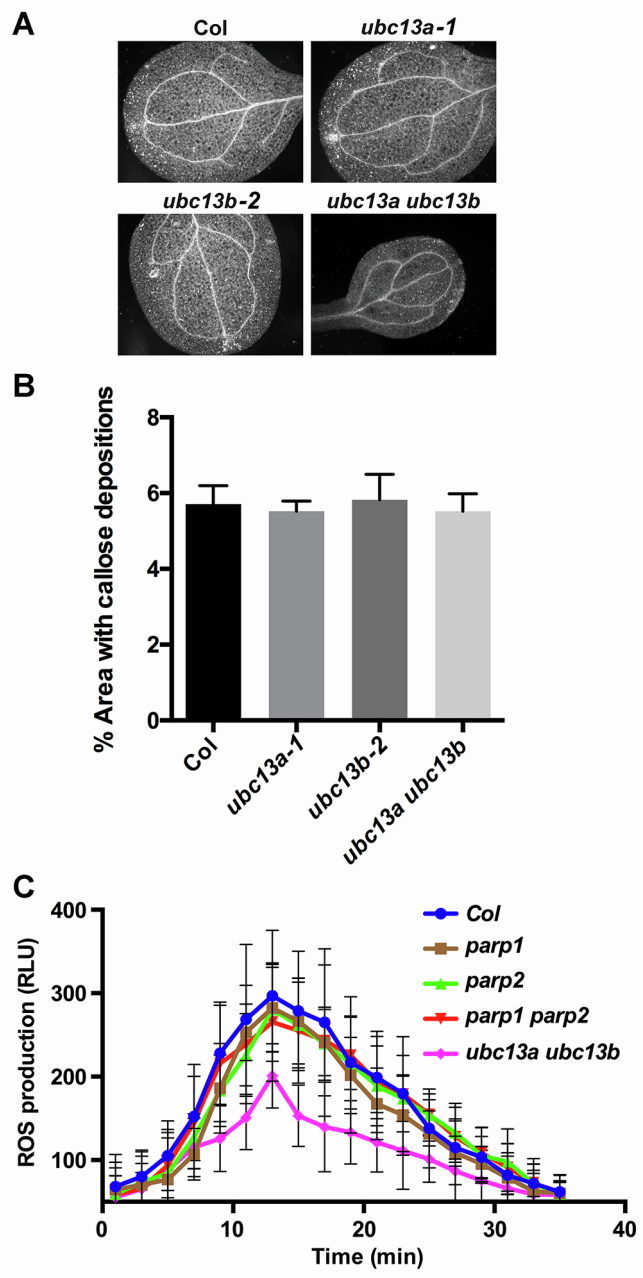

Supplemental Figure 5. PTI Response in the *parp* and *ubc13* Mutants.

(A) Flg22-induced callose deposition in *ubc13* mutants. Seven-day-old seedlings treated with 1 µM flg22 for 24 h were fixed and stained with aniline blue to highlight callose deposition. Representative images of callose deposition are shown.

(B) Quantification of callose deposition in (A). Data are shown as the mean ± SD (n = 12). Three independent experiments were carried out with similar results.

(C) Flg22-Induced ROS Production in the *parp* and *ubc13* Mutants. Leaf disks from 3-week-old plants were treated with 1 µM flg22 for 30 min. Data are shown as the mean ± SD (n = 12). Three independent experiments were carried out with similar results.

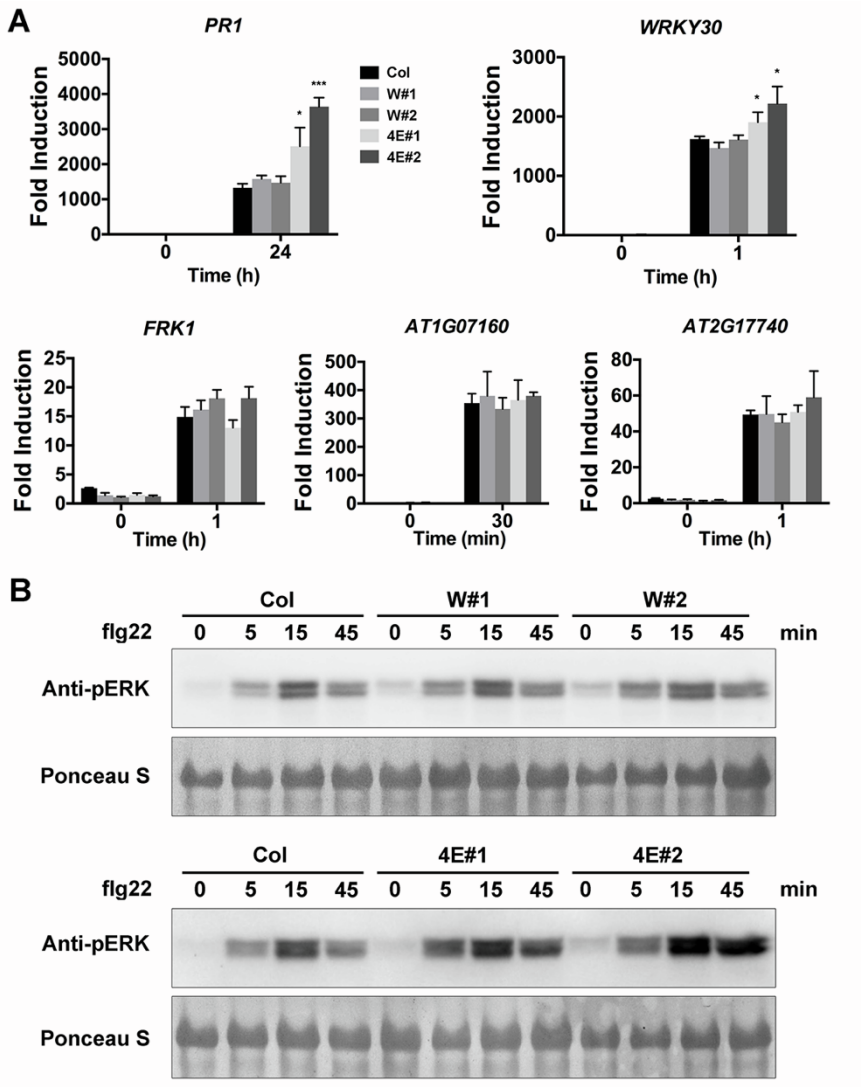

Supplemental Figure 6 . PTI responses in the *UBC13B^{4E}* lines.

(A) Flg22-induced defense marker gene expression in the *UBC13B^{4E}* lines. Ten-day-old *ProUBC13B:UBC13B-myc/ubc13a ubc13b* (W#1 and W#2) or *ProUBC13B:UBC13B^{4E}-myc*/*ubc13a ubc13b* (4E#1 and 4E#2) lines were treated with 1 μM flg22 for the indicated times and subjected to qRT-PCR analysis. Data are shown as the mean ± SD (n =3). Asterisk indicates a significant difference from Col (ANOVA, Tukey's pairwise comparisons, *$P < 0.05$, ***$P < 0.001$).

(B) Flg22-induced MAPK activation in the *UBC13B^{4E}* lines. Ten-day-old *UBC13B/ubc13a ubc13b* or *UBC13B^{4E}*/*ubc13a ubc13b* lines were treated with 1 μM flg22 and collected at 0, 5, 15, and 45 min after treatment. MAPK activation was detected by Western blot with anti-pERK antibody. Equal loading was confirmed by Ponceau S staining.

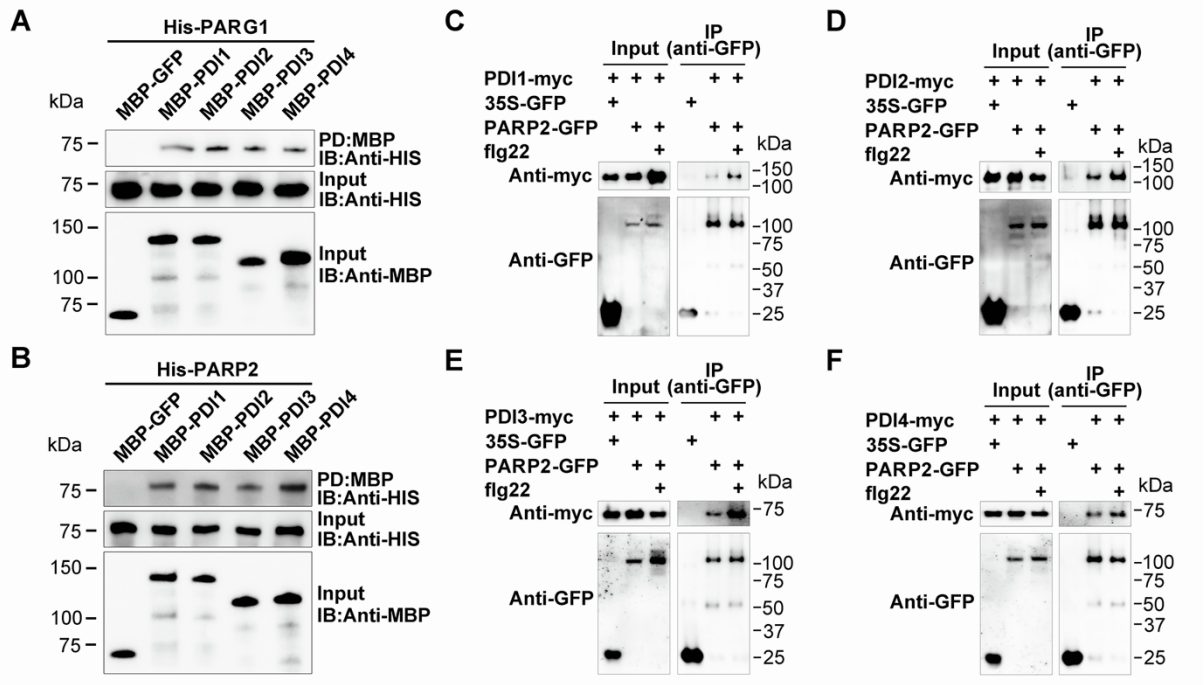

Supplemental Figure 7. PDIs Interact with PARG1 and PARP2 *In Vitro* and *In Vivo*.

(A) PARG1 interacts with PDI1, PDI2, PDI3, and PDI4 *in vitro*. HIS-tagged PARG1 was incubated with immobilized MBP-tagged GFP, PDI1, PDI2, PDI3, or PDI4 proteins. The input samples and immunoprecipitated fractions were detected by anti-HIS or anti-MBP antibody.

(B) PARP2 interacts with PDI1, PDI2, PDI3, and PDI4 *in vitro*. HIS-tagged PARP2 was incubated with immobilized MBP-tagged GFP, PDI1, PDI2, PDI3, or PDI4 proteins. The input samples and immunoprecipitated fractions were detected by anti-HIS or anti-MBP antibody.

(C-F) PARP2-GFP was coexpressed with myc-tagged PDI1, PDI2, PDI3, and PDI4 in *N. benthamiana*. Total proteins were extracted, immunoprecipitated with GFP-Trap magnetic beads, and immunoblotted with anti-myc or anti-GFP antibody. Plants were treated without or with 1 μM flg22 for 1 h.

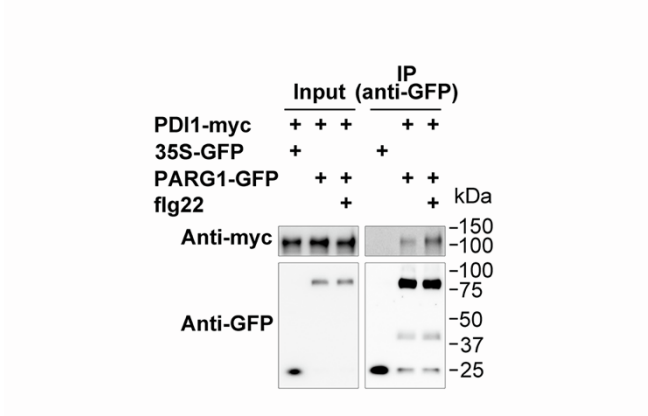

Supplemental Figure 8. PDI1 Interacts with PARG1 in Arabidopsis. PARG1-GFP was coexpressed with PDI1-myc in Arabidopsis protoplasts. Total proteins were extracted, immunoprecipitated with GFP-Trap magnetic beads, and immunoblotted with anti-myc or anti-GFP antibody. Protoplasts were treated without or with 1 μM flg22 for 1 h.

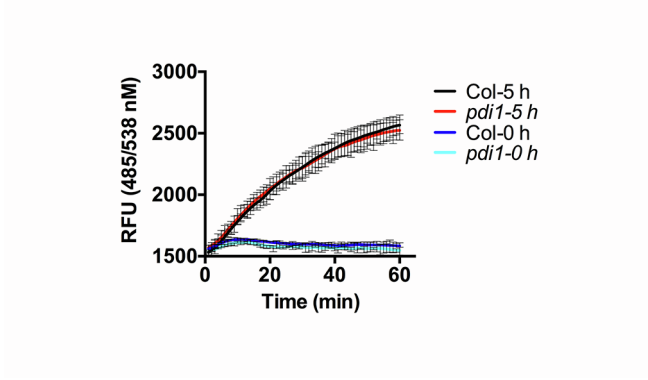

Supplemental Figure 9. Total PDI Activity in Col and *pdi1*. Ten-day-old seedlings of Col and the *pdi1* mutant were treated with or without 10 mM DTT for 5 h and subjected to protein disulfide isomerase assays. Data are shown as the mean ± SD of three biological replicates.

Supplemental Table 1. The List of Identified PARylated Sites in PARP2 and UBC13B.

Proteins	Confidence	Annotated Sequence	Modifications	# PSMs	Master Protein Accessions	Positions in Master Proteins
PARP2	High	[K].SYTWLEMDYGKEENDSPVNNDIPSSSSEVKPEQSK.[L]	1xHydroxamic_acid [E/D]	3	A0A178UW01	A0A178UW01 [254-288]
PARP2	High	[R].NSSNDTYESNK.[L]	1xHydroxamic_acid [E8]	1	A0A178UW01	A0A178UW01 [52-62]
PARP2	High	[K].SYTWLEMDYGK.[E]	1xHydroxamic_acid [E6]	1	A0A178UW01	A0A178UW01 [254-264]
PARP2	High	[R].LEEAIAEDTKK.[E]	1xHydroxamic_acid [E]	4	A0A178UW01	A0A178UW01 [32-42]
PARP2	High	[K].SYTWLEMDYGKEENDSPVNNDIPSSSSEVKPEQSK.[L]	1xHydroxamic_acid [E/D]	2	A0A178UW01	A0A178UW01 [254-288]
PARP2	High	[R].LEEAIAEDTKKEESK.[S]	1xHydroxamic_acid [E/D]	5	A0A178UW01	A0A178UW01 [32-46]
PARP2	High	[R].GDDVYDAILNQTNVR.[D]	1xHydroxamic_acid [D]	2	A0A178UW01	A0A178UW01 [165-179]
PARP2	High	[K].TAPNPSEAQTLEDGVVVPLGKPVER.[S]	1xHydroxamic_acid [D/E]	2	A0A178UW01	A0A178UW01 [579-603]
UBC13B	High	[K].LELFLPEEYPMAAPK.[VI]	2xHydroxamic_acid [E7; E8]	1	Q9FZ48	Q9FZ48 [56-70]
UBC13B	High	[K].LELFLPEEYPMAAPK.[VI]	1xHydroxamic_acid [E7]	1	Q9FZ48	Q9FZ48 [56-70]
UBC13B	High	[R].LLSEPAPGISASPSEENMR.[Y]	3xHydroxamic_acid [E4; E15; E16]	1	Q9FZ48	Q9FZ48 [17-35]
UBC13B	High	[R].LLSEPAPGISASPSEENMR.[Y]	2xHydroxamic_acid [E4; E15]	3	Q9FZ48	Q9FZ48 [17-35]
UBC13B	High	[R].LLSEPAPGISASPSEENMR.[Y]	1xHydroxamic_acid [E4]	9	Q9FZ48	Q9FZ48 [17-35]

Protein FDR Confidence: High (1% False Discovery Rate), Medium (5% False Discovery Rate), or Low (>5% False Discovery Rate).

Master: If more than one protein in a group has the same score, and equal number of PSMs, and an equal number of peptides, the protein with the longest sequence is designated as the master protein.

Accession: Protein accession number (from UniProtKB).

PSMs: Number of Peptide Spectrum Matches, or the number of spectra assigned to peptides that contributed to the inference of the protein.

Supplemental Table 2. The List of Identified PARylated Sites in PARP2 and PDI Proteins.

Proteins	Confidence	Annotated Sequence	Modifications	# PSMs	Master Protein Accessions	Positions in Master Proteins
PARP2	High	[K].KGAAVLDQWIPDEIK.[S]	1xHydroxamic_acid [E/D]	3	A0A178UW01	A0A178UW01 [142-156]
PARP2	High	[K].SYTWLEMDYGKEENDSPVNNDIPSSSSEVKPEQSK.[L]	1xHydroxamic_acid [E/D]	6	A0A178UW01	A0A178UW01 [254-288]
PARP2	High	[R].LEEAIAEDTKKEESK.[S]	1xHydroxamic_acid [E/D]	6	A0A178UW01	A0A178UW01 [32-46]
PARP2	High	[R].NSSNDTYESNK.[L]	1xHydroxamic_acid [E8]	3	A0A178UW01	A0A178UW01 [52-62]
PARP2	High	[K].TAPNPSEAQTLEDGVVVPLGKPVER.[S]	1xHydroxamic_acid [E7]	1	A0A178UW01	A0A178UW01 [579-603]
PARP2	High	[K].GMLLYNEYIVYNVEQIK.[M]	1xHydroxamic_acid [E7]	1	A0A178UW01	A0A178UW01 [608-624]
PARP2	High	[R].LCNDANNVSNAPVK.[S]	1xHydroxamic_acid [D4]	5	A0A178UW01	A0A178UW01 [99-112]
PDI1	High	[R].LEDDLSFYQTASPDIAK.[L]	1xHydroxamic_acid [D/E]	5	A0A178VF09	A0A178VF09 [248-264]
PDI1	High	[K].LFEIETQVK.[R]	1xHydroxamic_acid [E5]	2	A0A178VF09	A0A178VF09 [265-273]
PDI1	High	[K].TLAEDFLADK.[L]	1xHydroxamic_acid [E4]	1	A0A178VF09	A0A178VF09 [412-421]
PDI1	High	[K].SFDPIAVDVDR.[T]	1xHydroxamic_acid [D10]	1	A0A178VF09	A0A178VF09 [522-532]
PDI3	High	[K].YLLESDPSPNSIEEFCSGLAHGTVSR.[Y]	1xHydroxamic_acid [E]	4	A3KPF5	A3KPF5 [379-404]
PDI3	High	[R].VIDGNEFVMVLGYAPWCAR.[S]	2xHydroxamic_acid [D3; E6]	6	A3KPF5	A3KPF5 [90-108]
PDI3	High	[R].VIDGNEFVMVLGYAPWCAR.[S]	1xHydroxamic_acid [E/D]	6	A3KPF5	A3KPF5 [90-108]
PDI3	High	[K].SEPVPDNDNASIVTVVGK.[T]	2xHydroxamic_acid [D6; D8]	1	D7KIR0	D7KIR0 [408-425]
PDI3	High	[K].SEPVPDNDNASIVTVVGK.[T]	1xHydroxamic_acid [D]	5	D7KIR0	D7KIR0 [408-425]
PDI4	High	[K].LLFPNLKTNNVFVGLVKTEAEKYTSYDGPCQAEK.[I]	1xHydroxamic_acid [D/E]	2	Q66GQ3	Q66GQ3 [244-277]
PDI4	High	[R].SSDVAVEAGSEEELDDLEQLLAVDEQLQEERPEQQSEAETVSK.[A]	1xHydroxamic_acid [D/E]	7	Q66GQ3	Q66GQ3 [30-72]
PDI4	High	[K].TDDFESLAQPLEDIAR.[K]	1xHydroxamic_acid [D]	2	Q66GQ3	Q66GQ3 [316-331]
PDI4	High	[K].YLLESDPSPSNIEEFCFGLAHGTVSAYYK.[S]	1xHydroxamic_acid [E14]	2	Q66GQ3	Q66GQ3 [378-406]
PDI4	High	[KR].SSENVLLEVHTPWCINCEALSK.[Q]	1xHydroxamic_acid [E18]	5	Q66GQ3	Q66GQ3 [433-454]
Protein FDR Confidence: High (1% False Discovery Rate), Medium (5% False Discovery Rate), or Low (>5% False Discovery Rate).						
Master: If more than one protein in a group has the same score, and equal number of PSMs, and an equal number of peptides,						
the protein with the longest sequence is designated as the master protein.						
Accession: Protein accession number (from UniProtKB).						
PSMs: Number of Peptide Spectrum Matches, or the number of spectra assigned to peptides that contributed to the inference of the protein.						

Supplemental Table 3. The List of Primers Used in This Study.

Primers for T-DNA knockout lines				
AGI	**Mutant**	**T-DNA lines**	**LP primer**	**RP primer**
AT1G78870	*ubc13a-1*	WiscDsLox323H12	AAATGTGTTCTTGGTTGGTGG	ACACAACCAAAGACATGCTCC
AT1G16890	*ubc13b-2*	GABI-836B11	CAAGGCAGATTCTTCCAAGC	GGATAAGTGCGTCTCCATCAG
AT1G16890	*ubc13b-1*	SALK_047381	GCGTGGACCGCTTGCTGCAACT	ATCGAGTCATCGAGATCATGG
qRT-PCR primers				
Genes	**Forward primer**		**Reverse primer**	
UBC13A	ATGGCCAACAGTAATTTGCCG		TCATGCGCCGCTTGCATAAAG	
UBC13B	ATGGCCAATAGTAATCTTCCC		TTAAGCACCACTTGCGTAAAG	
PR1	AGAGGCAACTGCAGACTCAT		GTGTTCGCAGCGTAGTTGTA	
WRKY30	GCAGCTTGAGAGCAAGAATG		AGCCAAATTTCCAAGAGGAT	
FRK1	ATC TTCGCTTGGAGCTTCTC		TGCAGCGCAAGGACTAGAG	
At1G07160	CGTGTTGGGGATTGATTCG		AGAGCTCGGGCGGTTATG	
At2G17740	TGCTCCATCTCTCTTTGTGC		ATGCGTTGCTGAAGAAGAGG	
BiP1/2	ATATGGCTCGCTCGTTTGG		GGTTTCCTTGGTCATTGGCA	
BiP3	CACGGTTCCAGCGTATTTCAAT		ATAAGCTATGGCAGCACCCGTT	
UBQ5	GGAATCGACGCTTCATCTCG		ACTCCTTCCTCAAACGCTGA	
Primers for UBC13B mutants				
Redidues mutated to A			**Forward primer**	**Reverse primer**
E39, E40			TAACATTGAAATATCTCATATTTGCCGCTGATGGAGACGCACTTATCCC	GGGATAAGTGCGTCTCCATCAGCGGCAAATATGAGATATTTCAATGTTA
E71, E72			GGAGCTGCCATAGGATATGCTGCAGGCAAAAAGAGCTCCA	TGGAGCTCTTTTTGCCTGCAGCATATCCTATGGCAGCTCC
Primers for yeast two-hybrid				
Genes	**Forward primer**		**Reverse primer**	
PARP1	GGGGACAAGTTTGTACAAAAAAGCAGGCTTAATGGCAAGCCCACATAAGCC		GGGGACCACTTTGTACAAGAAAGCTGGGTCTCTCTTGTGCTTAAACCTT	
PARP2	GGGGACAAGTTTGTACAAAAAAGCAGGCTTAATGGCGAACAAGCTCAAAGT		GGGGACCACTTTGTACAAGAAAGCTGGGTCGTGCTTGTAGTTGAATTTGAC	
PARG1	GGGGACAAGTTTGTACAAAAAAGCAGGCTTAATGGAGAATCGCGAAGATCTTAAC		GGGGACCACTTTGTACAAGAAAGCTGGGTCAGGCGGCTGGATAGCTTTGTTGGTG	
PARG2	GGGGACAAGTTTGTACAAAAAAGCAGGCTTAATGGAACTGAGGGCAGATCTTAGG		GGGGACCACTTTGTACAAGAAAGCTGGGTCGGTAGACAGTGAGGTCATGAGCC	
PARP1-N	GGGGACAAGTTTGTACAAAAAAGCAGGCTTAATGGCAAGCCCACATAAGCC		GGGGACCACTTTGTACAAGAAAGCTGGGTCTTGTTCCCAAGATTCCCATG	
PARP2-N	GGGGACAAGTTTGTACAAAAAAGCAGGCTTAATGGCGAACAAGCTCAAAGT		GGGGACCACTTTGTACAAGAAAGCTGGGTCTTGCTGGTAGTGATAATATA	
UBC13A	GGGGACAAGTTTGTACAAAAAAGCAGGCTTAATGGCCAACAGTAATTTGCCG		GGGGACCACTTTGTACAAGAAAGCTGGGTCTCATGCGCCGCTTGCATAAAG	
UBC13B	GGGGACAAGTTTGTACAAAAAAGCAGGCTTAATGGCCAATAGTAATCTTCCC		GGGGACCACTTTGTACAAGAAAGCTGGGTCTTAAGCACCACTTGCGTAAAG	
BIP2	GGGGACAAGTTTGTACAAAAAAGCAGGCTTAAAAGAAGAGGCTACGAAGT		GGGGACCACTTTGTACAAGAAAGCTGGGTCGAGCTCATCGTGAGACTCAT	
SEC61	GGGGACAAGTTTGTACAAAAAAGCAGGCTTAATGGTGGGAAGTGGAGCTCC		GGGGACCACTTTGTACAAGAAAGCTGGGTCTTTGACAAAGTAGAGCTT	
SYP132	GGGGACAAGTTTGTACAAAAAAGCAGGCTTAATGAACGATCTTCTGAAGGG		GGGGACCACTTTGTACAAGAAAGCTGGGTCTTTTCTTGAGTTCTTCTGCAAG	
SYP122	GGGGACAAGTTTGTACAAAAAAGCAGGCTTAATGAACGATCTTCTCTCCGG		GGGGACCACTTTGTACAAGAAAGCTGGGTCCTTCCGTGTGTTCTTCTGATAA	
PDI1	GGGGACAAGTTTGTACAAAAAAGCAGGCTTAATGGAGAATGCGTCCAGTGGATC		GGGGACCACTTTGTACAAGAAAGCTGGGTCCAACTCATCCTTGGAACTAT	
PDI2	GGGGACAAGTTTGTACAAAAAAGCAGGCTTAATGGCTGACTCACTCTCTTCCTC		GGGGACCACTTTGTACAAGAAAGCTGGGTCCAATTCGTCCTTCGAGTCAC	
PDI3	GGGGACAAGTTTGTACAAAAAAGCAGGCTTAATGTCACCCGATTCCAATGTCG		GGGGACCACTTTGTACAAGAAAGCTGGGTCCAATTCATCTTTAGCAGACCC	
PDI4	GGGGACAAGTTTGTACAAAAAAGCAGGCTTAATGTCTGATGTCGCCGTCGAAGC		GGGGACCACTTTGTACAAGAAAGCTGGGTCTAACTCATCTTTACCAGACT	
PDI5	GGGGACAAGTTTGTACAAAAAAGCAGGCTTAGAAGAGACGGAGACGAAGGAG		GGGGACCACTTTGTACAAGAAAGCTGGGTCGAGCTCATCCTTGACTTCCTC	
PDI6	GGGGACAAGTTTGTACAAAAAAGCAGGCTTAATGGAGGAGACGAAGGAATTTGT		GGGGACCACTTTGTACAAGAAAGCTGGGTCCAGCTCGTCCTTTGCGGCCG	
PDI7	GGGGACAAGTTTGTACAAAAAAGCAGGCTTAATGGTGTCCACGAGCAAGAT		GGGGACCACTTTGTACAAGAAAGCTGGGTCGAAGTTTTTACCAAGTTCTA	
PDI8	GGGGACAAGTTTGTACAAAAAAGCAGGCTTAATGTCGTCAGATGATCAATTCAC		GGGGACCACTTTGTACAAGAAAGCTGGGTCGTCCTCTTTTTTGTCACTAG	
PDI9	GGGGACAAGTTTGTACAAAAAAGCAGGCTTAATGCTTTATGGATCTTCGTCACC		GGGGACCACTTTGTACAAGAAAGCTGGGTCCAACTCATCCTTAGAACCAA	
PDI10	GGGGACAAGTTTGTACAAAAAAGCAGGCTTAATGCTCTATGGATCTTCGTCGCC		GGGGACCACTTTGTACAAGAAAGCTGGGTCCAAGTCGTCCTTGGACTCAG	
PDI11	GGGGACAAGTTTGTACAAAAAAGCAGGCTTAGACGATGTGGTTGTTTTGACT		GGGGACCACTTTGTACAAGAAAGCTGGGTCAGAAGAAGCAACGAACGTGG	